8-2014

Exploration of the Validity of the Two-Dimensional Sagittal Plane Standing Long Jump Model

Lauren Hickox
Grand Valley State University

ScholarWorks Citation

Hickox, Lauren, "Exploration of the Validity of the Two-Dimensional Sagittal Plane Standing Long Jump Model" (2014). *Masters Theses*. 722.
https://scholarworks.gvsu.edu/theses/722

Exploration of the Validity of the Two-Dimensional Sagittal Plane Standing Long Jump Model

Lauren Hickox

A Thesis Submitted to the Graduate Faculty of

GRAND VALLEY STATE UNIVERSITY

In

Partial Fulfillment of the Requirements

For the Degree of

Masters of Science in Engineering

Padnos College of Engineering and Computing

August 2014

Acknowledgements

I would like to thank my committee members for all of the time and effort they put into the completion of my thesis. I would particularly like to thank my advisor, Dr. Blake Ashby, for guiding and supporting me throughout the research, analysis, and writing of my thesis. He was a great source of knowledge on biomechanics and the standing long jump, along with being instrumental in the development of my interest in the field. I would like to thank Dr. Gordon Alderink for his expertise in the motion capture lab and assistance in data collection and Dr. Wendy Reffeor for her engineering perspective on my analysis and review of my writing. I would also like to thank the Statistical Consulting Center at Grand Valley State University for all of the time the staff spent working with me and providing me advice on the appropriate statistical models for my study.

Abstract

Most previous standing long jump studies have been based on the assumption of two-dimensional sagittal plane motion. The purpose of this study was to investigate the validity of this assumption. Standing long jump trials were collected using six adult male subjects. Each subject stood with a foot on each of two force plates and performed eight standing long jumps for maximal distance. Inverse dynamics analyses were performed for the two-dimensional (2D) and three-dimensional (3D) models and the joint moments, powers, and work values were compared. The differences between these models with respect to the validity of the common planar jumping assumption were analyzed.

Good agreement was observed between the 2D and 3D methods for the lower body, with little difference in the moments, power, and work for the ankle, knee, hip, and lower back. For the upper body, the moments and work were similar, however significant differences were observed in power generation resulting from the two methods. There were also significant moments and power generated about the abduction/adduction axis for the shoulder. An approximately equal amount of work was found to be performed about the abduction/adduction and flexion/extension axes at the shoulder. The 3D model was also found to capture significant differences between the left and right sides of the body that were not able to be observed with the 2D model.

The results of this study show that a planar motion assumption should be sufficient for most studies of the standing long jump. However, in cases where upper body motion is being studied or small increases in performances are vital, a 3D model may be more appropriate as it more accurately represents the motion of the upper body and is better able to show the differences in performance between the two sides of the body.

Table of Contents

List of Figures

List of Tables

1 Introduction

Most standing long jump studies, including previous studies at Grand Valley State University (Filush, 2012; Vlietstra, 2014), assume that the standing long jump is a sagittal plane activity in order to use a two-dimensional model (2D) instead of a three-dimensional (3D) model. This may not be an acceptable assumption for jumping activities, particularly those that include arm motion. This study will investigate the validity of this assumption by comparing the results of inverse kinematic and dynamic analyses using both 2D and 3D models. The objective of this study was to answer the following question:

> How significant are the differences between the results of inverse kinematic and dynamic analyses of a 2D model and a 3D model for the standing long jump?

To answer these questions, a human subject study was designed to analyze the standing long jump motion using both 2D and 3D models. The 2D model was based on the single plane assumption that all motion (rotation and translation) of the body occurs in planes parallel to the sagittal plane. Under this assumption, all forces lie in the sagittal plane and all moments are about axes perpendicular to the sagittal plane. During this study, a motion capture system was used to record positions of markers on the subjects' bodies. Two force plates were also used to collect 3D force and center of pressure data during takeoff. The internal joint moments, power, and net work for the two cases were then compared to determine how significant the differences in results were between the models. The effect that the single plane assumption has on the inverse kinematic and dynamic results for the standing long jump may influence decisions on what assumptions are used for future studies.

2 Background

The standing long jump is an important athletic skill that was a part of the Olympic Games in Ancient Greece and is still used in many demanding sports today. It also is used as a test for lower limb function and physical aptitude and is a good predictor of sprint performance (Mackala et al., 2013; Wakai and Linthorne, 2005). The standing long jump is an explosive movement that is difficult for many to perform as it requires proper technique and a high level of coordination (Aguado et al., 1997; Wakai and Linthorne, 2005).

There are three main phases that occur during the jump: takeoff, flight, and landing. Figure 1 shows these phases and the corresponding jump distances. During takeoff, the body leans forward in the direction of motion and during flight, the legs are swung forward for the landing phase. During the landing phase, the feet are generally ahead of the hips and the trunk is still leaning forward (Wakai and Linthorne, 2005). Takeoff is critical as a majority of the jump performance is determined in this phase. The goal at takeoff is to optimize the combination of vertical velocity and horizontal velocity to achieve the furthest jump distance (Hay et al., 1986). In flight, the objective is to prepare the body for landing. The technique used in landing can result in a small increase in performance (Aguado et al., 1997).

2.1 Factors that Affect Standing Long Jump Performance

There are many factors that affect performance in the standing long jump; some are related to the characteristics of the jumper and related to the technique or body position used during the jump. Characteristics of the jumper that affect performance are joint and muscular strength and functional symmetry (Mackala et al., 2013). They can be improved with time and effort but are not easily adjustable. Initial body position and techniques used can be adjusted to optimize performance. Initial body position includes starting posture, foot placement, and knee angle (Mackala et al., 2013). Control of takeoff angle and takeoff velocity is also important for maximum performance (Mackala et al., 2013; Wakai and Linthorne, 2005). Techniques include the use of countermovement during takeoff and the use of double-arm swing (Ashby and Heegaard, 2002; Wakai and Linthorne, 2005). Coordination between the motions of the upper and lower body, as in countermovement and arm swing, is another main factor in jump performance and in some cases is more critical to jump length than force production (Aguado et al., 1997; Wakai and Linthorne, 2005).

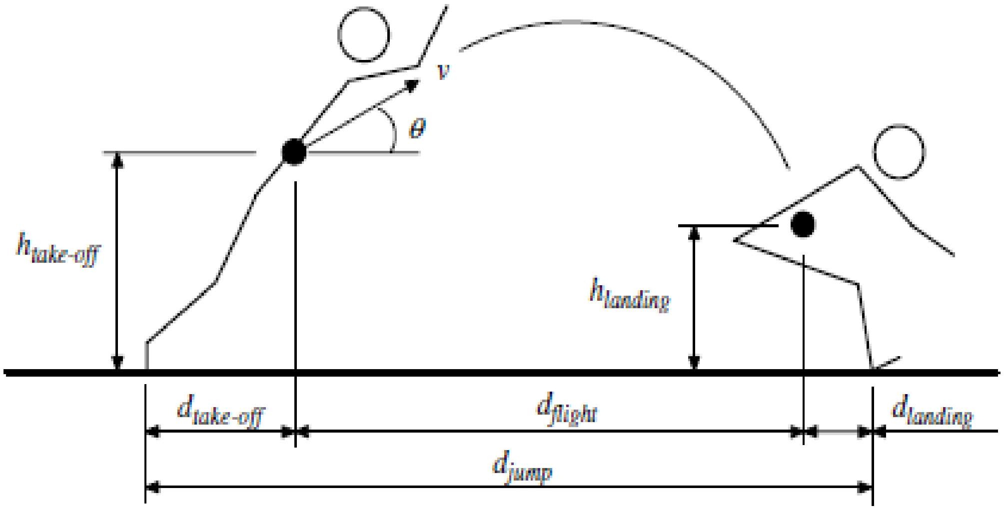

Figure 1: Phases and Jump Distance for the Standing Long Jump (Wakai and Linthorne, 2005).

2.2 3D Models in Jumping

A review of the literature revealed no studies that experimentally investigated jumping using a 3D model. However, simulations have been performed to optimize vertical jumping using a 3D full body model by Anderson and Pandy (1999), which added complexity compared to previous 2D models used for jumping simulations (Pandy et al., 1990). The 3D model had improved results in that it matched experimental data better than a 2D model. One of the main improvements was that the ground reaction forces were more accurate. Another important advantage was that the 3D model was able to predict movements of body segments in the frontal plane and transverse plane, instead of just the sagittal plane. However, the complexity of the 3D model increased the computational cost for the dynamic optimization solution. Faster computers could decrease the time to solution but it would still be time-consuming and computationally expensive (Anderson and Pandy, 1999).

2.3 Symmetry in Jumping

Along with planar movement, another related assumption used to simplify data collection and analysis in jumping studies is bilateral symmetry (Yoshioka et al, 2010). This may not be an accurate assumption as asymmetries are very common. A simulation study was performed by Yoshioka et al. (2010) on the effect of bilateral symmetry of muscle strength on countermovement vertical jump performance. The simulation resulted in very similar jumping heights for the symmetrical and asymmetrical models, indicating that the bilateral strength asymmetry did not significantly affect performance in this case. There was a compensation effect in the asymmetrical model as the center of mass of the body shifted laterally in order to distribute the load according to muscle strength of each leg. As the body may naturally compensate for asymmetry in many cases, overall similar performance is possible even though the kinematics and kinetics of the motion are different. The assumption of symmetry may cover up the important differences that cause or are caused by asymmetry. This may be a problem particularly where the standing long jump is used as a test of functionality or in athletic training. If the performance remains the same, weakness in a leg may not be discovered (Yoshioka et al, 2010). Analyses of jumping or other movements using the symmetry assumption may neglect important parts of the motion and result in incorrect conclusions.

2.4 Model Selection

There are trade-offs when selecting which model to use for a study. 3D models may more accurately represent the motion being studied, but it will add complexity and come at the cost of processing and analysis time. This study experimentally investigated the differences between a 2D and 3D model for the case of the standing long jump. Gaining a better understanding of the differences between the two types of models should help with correct model selection for a specific application in future studies.

3 Description of Models

For this study, 2D and 3D full-body models were created under the following assumptions:

1. Segment lengths are constant during the jumping motion.
2. The center of mass of each segment is located on the segment long axis.
3. The center of mass and moments of inertia remain constant with respect to anatomical reference frames of the segments.
4. The principle axes of inertia are aligned with the anatomical coordinate axes for each segment (The anatomical coordinate systems were defined to match the frontal, transverse, and sagittal planes of each segment for which the inertial parameters were given).

The 2D model also includes the assumptions of sagittal plane motion and bilateral symmetry. The models were designed to align as closely as possible with the same joint centers and the long axis of each anatomical reference frame for the 3D model matching the corresponding 2D segment.

3.1 Marker Set

A marker set was developed that could be used for both 2D and 3D full body kinematics. Markers were placed at the anatomical locations required to determine joint centers and to create anatomical reference frames for each segment in a 3-dimensional, 12-segment full body model as shown in Figure 2. The anatomical reference frames used for this model were based on Ren et al. (2008) and recommendations by the International Society of Biomechanics (ISB) (Wu et al., 2002; Wu et al., 2005).

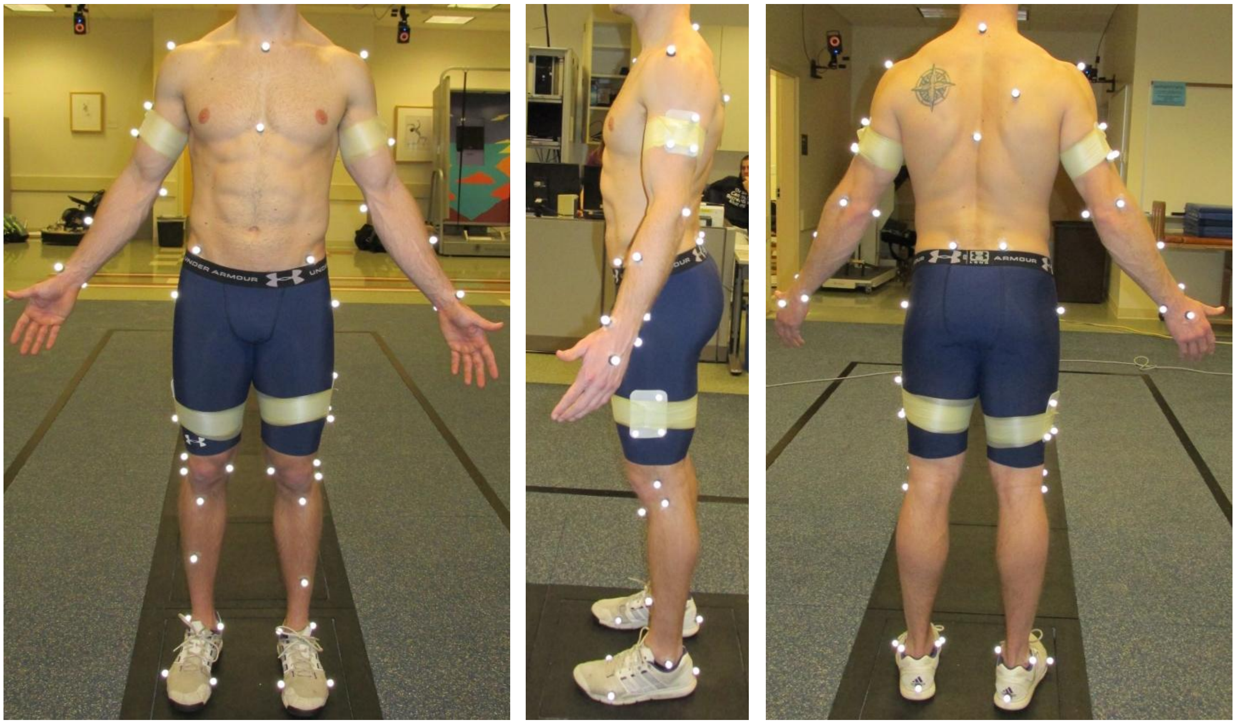

Figure 2: Front, Right Side, and Back Views of Marker Placement on Subject.

Clusters of three markers were also included on the thigh and upper arm segments for the determination of the hip and shoulder joint centers. Markers were added on the greater trochanter and acromion process on both sides of the body as reference points for the hip and shoulder joint centers. An additional marker was included on the right shoulder blade to make the marker set asymmetrical for ease of labeling and processing. The marker on the right shoulder blade was also used to create a trunk technical reference frame to fill gaps in trials in which the sternum or clavicle markers dropped out. Bony landmarks were used for as many marker locations as possible to increase accuracy of placement and to reduce soft tissue artifact. The full marker set is shown in Table 1.

Table 1: Full Marker Set for 2D and 3D Models.

Marker Name	Location
Left Lower Extremity	
LGRTR	Greater Trochanter
LTHI1	Left Thigh 1
LTHI2	Left Thigh 2
LTHI3	Left Thigh 3
LLKNE	Left Lateral Femoral Epicondyle
LMKNE	Left Medial Femoral Epicondyle
LSHN	Left Anterior Crest of Tibia
LTUB	Left Tibial Tuberosity
LFBH	Left Fibular Head
LLML	Left Lateral Malleolus
LMLL	Left Medial Malleolus
LHEE	Left Heel
LMT1	Left Head of 1st Metatarsal
LMT5	Left Head of 5th Metatarsal
Right Lower Extremity	
RGRTR	Right Greater Trochanter
RTHI1	Right Thigh 1
RTHI2	Right Thigh 2
RTHI3	Right Thigh 3
RLKNE	Right Lateral Femoral Epicondyle
RMKNE	Right Medial Femoral Epicondyle
RSHN	Right Anterior Crest of Tibia
RTUB	Right Tibial Tuberosity
RFBH	Right Fibular Head
RLML	Right Lateral Malleolus
RMLL	Right Medial Malleolus
RHEE	Right Heel
RMT1	Right Head of 1st Metatarsal
RMT5	Right Head of 5th Metatarsal
Pelvis	
LASI	Left Anterior Superior Iliac Spine
RASI	Right Anterior Superior Iliac Spine
LPSI	Left Posterior Superior Iliac Spine
RPSI	Right Posterior Superior Iliac Spine

Marker Name	Location
Trunk	
CLAV	Jugular Notch
STRN	Xyphoid Process
T8	Mid-lower Back
C7	7th Cervical Vertebra
LACR	Left Acromion Process
RACR	Right Acromion Process
RBAK	Right Shoulder Blade
Left Upper Extremity	
LUS	Left Ulnar Styloid
LRS	Left Radial Styloid
LFRM	Left Forearm (Lateral Side)
LLE	Left Lateral Epicondyle
LME	Left Medial Epicondyle
LUA1	Left Upper Arm 1
LUA2	Left Upper Arm 2
LUA3	Left Upper Arm 3
Right Upper Extremity	
RUS	Right Ulnar Styloid
RRS	Right Radial Styloid
RFRM	Right Forearm (Lateral Side)
RLE	Right Lateral Epicondyle
RME	Right Medial Epicondyle
RUA1	Right Upper Arm 1
RUA2	Right Upper Arm 2
RUA3	Right Upper Arm 3
Total: 55 markers	

3.2 3D Model

The 12 segments used in the 3D model for this study were the feet, shanks, thighs, pelvis, trunk, upper arms, and forearms. The pelvis and trunk were assumed to be two separate segments, separated at the joint between the third and fourth lumbar vertebrae (L3/L4). The trunk segment consisted of the head, neck, upper trunk, and midtrunk, and the hands were included in the forearm segments. The joint center definitions are shown in Table 2 and the segment definitions are shown in Table 3. The joints were numbered starting from 1 at the left ankle and going up to 13 at the right wrist. The same joint numbers were used for the 2D and 3D models. An anatomical reference frame was assigned to each segment. Descriptions of these reference frames are shown in Appendix A. The coordinate system directions are common among the anatomic reference frames. In the neutral (anatomic) position, all x-axes point in the anterior direction, all y-axes are along the long axis of the segment and point in the superior direction, and all z-axes point towards the right.

Table 2: Joint Center Definitions.

Joint	**Number** (Left,Right)	**Definition**
Ankle (AJC)	1,2	Midpoint between LML and MML
Knee (KJC)	3,4	Midpoint between LKNE and MKNE
Hip (HJC)	5,6	Functional center of rotation
Lower Back (LBJC)	7	Based on anthropometric data for average male
Shoulder (SJC)	8,9	Functional center of rotation
Elbow (EJC)	10,11	Midpoint between LE and ME
Wrist (WJC)	12,13	Midpoint between RS and US

Table 3: 3D Segment Definitions.

Segment		Proximal Endpoint	Distal Endpoint
foot		HEE	Midpoint between MT1 and MT5 (midMT)
shank		KJC	AJC
thigh		HJC	KJC
pelvis		LBJC	Midpoint between HJCs (midHJC)
trunk	midtrunk	STRN*	LBJC
	upper trunk	C7*	STRN*
	head	C7*	Top of Head
upper arm		SJC	EJC
forearm	lower arm	EJC	WJC
	hand	WJC	3rd Metacarpal (MET3)

*projected on y-axis of trunk anatomic reference frame (LBJC to midpoint between CLAV and C7)

3.3 2D Model

The 2D link-segment model contained seven segments: foot, shank, thigh, pelvis, trunk, upper arm, and forearm. Bilateral symmetry was assumed for marker positions and the markers on only one side of the body were used for the 2D model. The segment endpoints, mostly joint centers, were found for the 3D model and then projected onto the sagittal plane (x-z plane in the lab global coordinate system). These 2D positions of the endpoints were used to calculate segment angles. A diagram of the joints and segments in the 2D model are shown in Figure 3(a). The joint angles are shown in Figure 3(b).

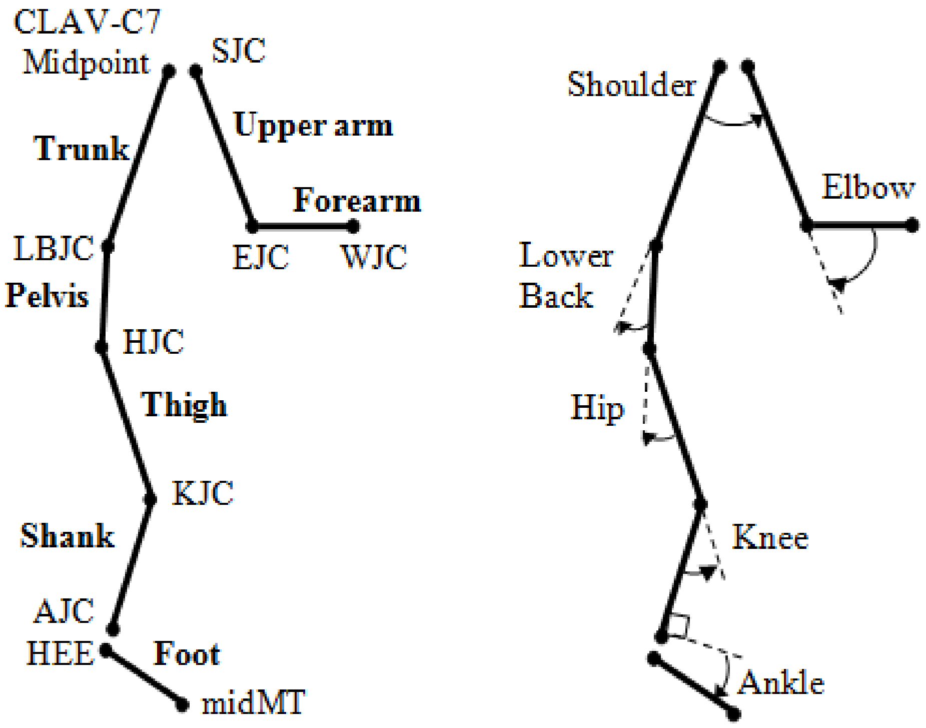

(a) (b)

Figure 3: 2D Model for Comparison of Flexion/Extension Angles: (a) Endpoints and Segments (segment names bolded) and (b) Joint Angles (arrows pointing towards positive joint motion in the 2D sign convention)

3.4 Body Segment Parameters

The body segment parameters used in this study, including length (L), mass (m), center of mass (CoM) location, and moment of inertia (I), were based on the segment definitions and parameters from Zatsiorsky et al. (1990) and adapted by de Leva (1996) to use joint centers as segment endpoints. The original study by Zatsiorsky et al. (1990) used a sample of 100 young adult males (mean age of 24) which aligns well with the subjects used in this study. These parameters are shown in Table 4.

Table 4: Body Segment Inertial Parameters (de Leva, 1996).

Segment		**Mass** (% body mass)	**Distance to CoM from Proximal Endpoint** (% segment length)	**Radii of Gyration about CoM** (% segment length)		
				ρ_x	ρ_y	ρ_z
foot		1.37	44.15	12.40	24.50	25.70
shank		4.33	43.95	24.60	10.20	25.10
thigh		14.16	40.95	32.90	14.90	32.90
pelvis		11.17	61.15	55.10	58.70	61.50
trunk	midtrunk	16.33	45.02	46.80	38.30	48.20
	upper trunk	15.96	50.66	46.50	32.00	50.50
	head	6.94	49.98	31.50	26.10	30.30
upper arm		2.71	57.72	26.90	15.80	28.50
forearm	lower arm	1.62	45.74	26.50	12.10	27.60
	hand	0.61	79.00	51.30	40.10	62.80

For each subject, data were collected during a static trial and used to determine the segment parameters. Two static trials were captured while the subject was standing in the anatomic position with one trial on each force plate. The total mass of each subject was calculated by averaging the masses resulting from the static trials on the force plates. Segment lengths were calculated by finding the distance between joint centers in the 3D position data from the first static trial. The lengths for the feet, hands, and head of each subject were not calculated. Average values for young adult males corresponding to the segment inertial parameters in this study were used for these lengths. The average foot length was 258.1 mm, the average hand length was 86.2 mm, and the average head length was 242.9 mm (de Leva, 1996). The same segment lengths were used for both the 2D and 3D analyses.

In Table 4, the radii of gyration about the CoM (ρ) are given about each axis of the segment anatomical reference frame. For each segment, the moment of inertia about each axis was determined using equation (1) (Winter, 1990). The moment of inertia about the z-axis of the anatomical reference frame was used for the 2D model.

$$I = m\rho^2 \tag{1}$$

The head, upper part of trunk, and middle part of trunk were merged into one trunk segment and a combined segment length, mass, center of mass, and moments of inertia were determined. The body segment parameters were also combined for the hand and lower arm to form a single forearm segment. For the 2D model, the masses and moments of inertia were doubled for the extremities.

4 Determination of Joint Centers

The ability to determine accurate joint centers is critical to the kinematic and kinetic analysis of joint motion. However, the exact locations of many joint centers are difficult to determine, particularly with ball joints such as the hip joint. Many methods have been used to determine the hip joint center (Camomilla et al., 2006; Capozzo, 1984; Cereatti et al., 2009; Davis et al., 1991; Delonge, 1972; Ehrig et al., 2006; Gamage and Lasenby, 2002; Halvorsen, 2003; Harrington et al., 2007; Holzreiter, 1991; Kasa, 1976; Leardini et al., 1999; Lopomo et al, 2010; MacWilliams, 2008; Marin et al., 2003; Pratt, 1987; Sangeux et al., 2011; Schwartz and Rozumalski, 2005; Stoddart et al., 1999; Woltring et al., 1985). MRIs and other medical imaging software can be used to find very accurate joint centers but they are not practical in many clinical and research settings. Joint centers can also be estimated using regression (predictive) methods or functional (coordinate transformation) methods. Regression methods are based on empirical correlations and relate joint centers to palpated anatomical landmarks. Functional methods do not rely on empirical correlations; they rely on mathematical analysis of the motion of one or more segments about a center of rotation (CoR). Functional methods can be categorized as sphere fit techniques or transformation techniques (Ehrig et al., 2006).

After a review of the current methods used for ball joints and preliminary testing, as detailed in Appendix B, the SCoRE method was chosen for the hip and shoulder joint centers as it is both simple and accurate. It is one of the only methods that allows for motion of the segments on both sides of the joint and is capable of calculating a moving CoR (Ehrig et al., 2006).

4.1 Hip and Shoulder Joint Centers

In the SCoRE method, local reference frames are assigned to the segments on both sides of the appropriate joint using at least three markers placed on each segment. The global differences between the CoRs found in each local reference frame are minimized in order to determine the CoR locations in the local coordinate systems of each segment that best fit the collected marker data. Equation (2) shows the function that is minimized in the SCoRE method to determine the hip joint center:

$$f_{SCoRE}(c_1, c_2) = \sum_{i=1}^{n} \| R_i c_1 + t_i - (S_i c_2 + d_i) \|^2 \tag{2}$$

where c_1 and c_2 are the CoRs in the local coordinate systems, R_i and S_i are the rotation matrices from the global coordinate system to the segment local coordinate systems, and t_i and d_i are the locations of the local origins in the global coordinate system (Ehrig et al., 2006).

The function is minimized by writing it as a system of linear equations and turning it into a least squares problem as shown in equation (3) (Ehrig et al., 2006; Nikooyan et al., 2011). The least squares function (`lsqr`) in Matlab was used to solve equation (2) for the hip joint centers in the local coordinate systems (c_1 and c_2).

$$\begin{pmatrix} R_1 & -S_1 \\ \vdots & \vdots \\ R_n & -S_n \end{pmatrix} \begin{pmatrix} c_1 \\ c_2 \end{pmatrix} = \begin{pmatrix} d_1 - t_1 \\ \vdots \\ d_n - t_n \end{pmatrix} \tag{3}$$

For the hip joint center determination, segment 1 was considered to be the thigh segment with c_1 as the estimated position vector for the hip CoR in the local coordinate system of the thigh. R_i is the rotation matrix from the global coordinate system to the local thigh coordinate system at time i and t_i is the position vector for the local segment origin in the global coordinate system. Segment 2 was considered to be the pelvis segment with corresponding values for c_2, S_i, and d_i. The result of the SCoRE method is two local estimates for the hip joint CoR, one in the thigh coordinate system and one in the pelvis coordinate system. These local CoRs were transformed into the global coordinate system and the mean was taken of the two positions to determine the global CoR estimate for the hip joint.

With the SCoRE method, the motion used when collecting the marker data affects the accuracy of the resulting joint centers. Studies comparing hip joint centers determined using different motions have found that a combination of flexion/extension, abduction, and circumduction (FE/Abd/Circ) movements resulted in the most accurate joint centers for the hip (Begon, 2007; Camomilla, 2006). Different ranges of motion and numbers of cycles were also compared. It was found that 10 cycles of the FE/Abd/Circ movements with a limited range of motion resulted in the most accurate joint centers. Limited movements have an advantage over full movements as they cause less skin deformation and soft tissue artifact. However, ten cycles were required for this higher accuracy due to the limited motion. For a full range of motion, one cycle was sufficient as more positions were collected per cycle. In this case, increasing the number of cycles did not increase the accuracy. The FE/Abd/Circ movements at full range of motion were shown to have the highest accuracy for one cycle, only slightly lower than the accuracy of the case with limited motion and 10 cycles (Begon, 2007). For the purposes of this study, performing 10 cycles was not practical as this would have been very time consuming to complete for multiple joints and may have fatigued the subject prior to the jumping trials. Also, capturing a set of 10 movement cycles for each joint center would have generated a very large amount of data that would have been time consuming to process. Therefore, the motion that was used for this study was one cycle of the FE/Abd/Circ movements at full range of motion as it has high accuracy and was efficient to collect and process.

The SCoRE method was also applied to the shoulder as studies have shown that SCoRE is one of the most accurate and repeatable methods for determining the shoulder joint center in healthy subjects (Lempereur et. al, 2010; Monnet, 2007; Nikooyan, 2011). In this case, the upper arm was considered to be segment 1 and the trunk was considered to be segment 2. With respect to data collection methods, one cycle of the FE/Abd/Circ movements at full range of motion was also shown to have high accuracy for the shoulder joint center (Monnet, 2007; Nikooyan, 2011). Therefore, the same joint center estimation method and motion for collecting the required data was used for both the hip and shoulder joints.

4.2 Lower Back Joint Center

For the lower back, a virtual joint center was created with a method used by Clancy (2010) and based on the segment definitions and anthropometric data originally from Zatsiorsky et al. (1990) and modified by de Leva (1996) to use joint centers as segment endpoints. In these segment definitions, the lower part of the trunk (pelvis) is separated from the middle part of the trunk by the omphalion (navel), which is in approximately the same transverse plane as L3/L4 (Lariviere and Gagnon, 1999).

To determine the location of L3/L4 from the markers used in this study, an initial trunk long (y) axis from mid HJC to the midpoint between the CLAV and C7 markers was created for a static trial, during which the subject was standing in anatomical position. The lower back joint center was assumed to be located on this axis at a distance from the mid HJC endpoint corresponding to the average anthropometric data from Zatsiorsky et al. (1990) and adapted by de Leva (1996). According to segment definitions in de Leva (1996), the length of the full trunk (lower, middle, and upper parts) is defined by midHJC and C7 (projected on the long axis of the trunk). For the average male in the study by Zatsiorsky et al., the trunk length was 603.3 mm (as cited in de Leva, 1996). The end points for the pelvis (lower part of the trunk) were the L3/L4 (omphalion) and midHJC. The average length of this segment was 145.7 mm. Therefore, the location of the lower back joint center was 24.15% (145.7 mm / 603.3mm x 100%) of the trunk length from midHJC for the average young adult male as shown below:

$$\mathrm{LBJC} = \mathrm{midHJC} + 0.2415\,(\mathrm{C7}_{\mathrm{on\ trunk\ long\ axis}} - \mathrm{midHJC}) \quad (4)$$

4.3 Other Joint Centers

The joint centers for the ankle, knee, elbow, and wrist were assumed to be the midpoint between the medial and lateral joint markers. They were determined using equations (5) through (8) on the marker position data from one static trial (with marker names as described in Table 1). These joint centers were then averaged over the entire static trial and transformed into technical reference frames, to later be applied to the dynamic trials.

$$AJC = \frac{LML+MML}{2} \quad (5)$$

$$KJC = \frac{LKNE+MKNE}{2} \quad (6)$$

$$EJC = \frac{LE+ME}{2} \tag{7}$$

$$WJC = \frac{RS+US}{2} \tag{8}$$

5 Experimental Design

This study was designed to analyze the kinematics and kinetics of the standing long jump using 2D and 3D models. A motion capture system consisting of eight cameras, two force plates, and a set of reflective markers were used to collect the data. The reflective markers were placed on the upper and lower body and attached to the skin, clothing, and shoes of the subjects with double-sided tape (Figure 2). The marker positions were then documented with still photography. The subjects were instructed to jump from the force plates for maximum distance during each trial, with no restrictions on takeoff position or arm motion during the jump. The force plates captured the ground reaction forces and locations of the centers of pressure for each foot throughout the takeoff phase. The jumping trials were also recorded with video.

5.1 Subject Selection

Six adult male subjects (mean ± standard deviation, mass: 90.3 ± 12.0 kg and average height: 182.0 ± 6.3 cm) volunteered to participate in this study. All subjects were informed of the study requirements, along with the goals of the study and the risks involved, and gave their consent. Each subject completed a survey to ensure reasonable athletic ability and at least occasional physical activity. The survey also determined whether a subject had a history of injury that could increase the risks of the jumping activities required for the study. The protocol for the study was approved by the Human Research Review Committee at Grand Valley State University.

5.2 Equipment

Data for the jumping trials were captured using a Vicon motion capture system (Vicon Motion Systems Ltd., Los Angeles, CA) consisting of eight cameras and two in-ground AMTI force plates (Advanced Mechanical Technology Inc., Watertown, MA). The 3D locations of reflective markers placed on the body were recorded using the infrared LED strobe lights on each camera operating at 120 Hz. The force plates were used to capture the 3D ground reaction forces, moments, and the locations of the centers of pressure during the takeoff phase of each jump. The Vicon data station collected data from both the cameras and the force plates. The Vicon Nexus software at the data station was then used to process and export the position and force data for further analysis. The Vicon camera system was calibrated and the force plates were zeroed prior to each data collection session.

5.3 Data Collection

The subjects were asked to wear athletic shoes and shorts with no shirts (all subjects were male). The full marker set was placed on the skin, clothing, and shoes of each subject. Correct marker placement was checked by an experienced physical therapist. To increase jumping performance and reduce the risk of injury, the subjects performed a short warm-up by running on a treadmill at a self-selected speed for five minutes. Brief stretching was allowed if desired by the subjects.

A static trial was then collected as the subjects stood in anatomical position in the middle of the video capture volume. Trials consisting of leg and arm rotations were collected for use in the SCoRE method. The subjects performed one cycle of the FE/Abd/Circ movements for each hip and shoulder joint in separate trials. The subject performed three to four practice jumps to familiarize themselves with the motion, allowing for maximal effort to be put into the collected jumping trials. After the warm-up and practice, the subjects were asked to perform eight standing long jumps recorded by the motion capture system. For the jumping trials, the subjects were asked to stand with one foot on each force plate and jump as far as possible once given a verbal signal. The subjects were allowed to rest as long as desired between jumps.

6 Data Analysis

Using the Vicon system and Nexus 1.8.4 (Vicon Motion Systems Ltd., Los Angeles, CA) software, the kinematic and force data from the static and dynamic trials were captured, processed, and exported to CSV files. In Nexus, the model used for this study was applied to the data and all of the markers were labeled. A majority of the gaps in the marker data were filled with the spline fill (which uses a Woltring quintic spline function) and pattern fill (which linearly warps the motion of the source marker into the gap) tools in the software. All of the ghost markers in the trials were also removed.

The spreadsheets of data were then imported and analyzed using MatLab R2013a (Mathworks, Natick, MA) software. The force plate data was subsampled at a 1:10 ratio as the marker data was collected at 120 Hz and the force plate data was collected at 1200 Hz. The time where the ground reaction forces went to zero for both force plates was defined as takeoff (time = 0). The start of the jump cycle was defined as 1.2 seconds (144 frames) before takeoff. The data was clipped at these points, while leaving an extra frame of data on either end of the jump cycle to be used for calculating velocities and accelerations in the kinematic analysis.

There were still some gaps remaining in the marker data that were not able to be filled in Vicon Nexus, primarily in the trunk markers. Either the CLAV, STRN, or both markers were missing in almost every trial. Two trials had gaps in the T8 marker and one trial had a gap in the RBAK marker. On other segments, the LPSIS marker had a gap in one trial and the LTHI2 marker had a gap in one trial. To fill these gaps, technical reference frames were created with the remaining markers on a segment in a static trial. Markers that needed to be filled in the jumping trials were then transformed from the static trials into the appropriate technical reference frames. The same technical reference frames were created with the dynamic data and the missing marker positions were transformed from these technical reference frames into the global reference frames in each dynamic trial. In this way, a virtual marker was created for each of the markers with gaps in the dynamic trials. This virtual marker data was used to replace the entire jumping cycle of data for each marker with gaps. The original data for these markers was eliminated as just filling in the gaps with the virtual marker data would have resulted in jumps in the data and caused issues during the inverse kinematic and dynamic analyses. The impact that these gaps had on the results of this study was low due to the inverse dynamics method used. As described in sections 6.3 and 6.4, the equations of motion for the trunk segment were discarded so the errors in the trunk results due to the replaced markers did not carry over to the other segments.

The data were filtered to remove high frequency noise using a bidirectional, 4th order low pass Butterworth filter with a cutoff frequency of 10 Hz for both the marker position data and the force plate data. The filtered marker and force plate data for the jump cycles were then exported to new CSV files for each trial.

6.1 Kinematic Analysis for 3D Model

A custom program written in MatLab was used to analyze the marker position data and calculate the segment and joint angles for the static and dynamic trials. For the static data, technical reference frames were created for each segment. The joint centers were determined from the rotational and static data trials. These joint centers were averaged for all of the static data resulting in a single position for each joint center in the global reference frame and then transformed into technical reference frames for use in the dynamic trials.

For the dynamic trials, technical reference frames were created for each segment and used to determine the joint centers (from the static case) expressed with respect to the global reference frame. These joint centers along with other dynamic marker data were used to create anatomical reference frames for each segment as described in Appendix A. The rotation matrices for the anatomical reference frames were used to determine the joint rotation matrices using the equation:

$$R_{d/p} = \left(R_{d/G}\right)\left(R_{p/G}\right)^T \tag{9}$$

where $R_{d/p}$ is the joint rotation matrix from the proximal segment to the distal segment, $R_{d/G}$ is the segment rotation matrix from the global reference frame to the distal segment reference frame, and $R_{p/G}$ is the segment rotation matrix from the global reference frame to the proximal segment reference frame. Equations for the Euler angles at each joint were determined for an XYZ rotation order as shown in Appendix C. The Euler angle equations and the joint rotation matrices were used to calculate the three angles at each joint (Table 5). The sign convention used in this study is also shown.

Table 5: Description of 3D Angles at Each Joint.

Joint	**Motion about x-axis (-/+)**	**Motion about y-axis (-/+)**	**Motion about z-axis (-/+)**
Ankle	Inversion/Eversion	Internal/External Rotation	Dorsiflexion/Plantarflexion
Knee	Varus/Valgus	Internal/External Rotation	Flexion/Extension
Hip	Adduction/Abduction	Internal/External Rotation	Flexion/Extension
Lower Back	Left/Right Bend (of upper body)	Left/Right Rotation (of upper body)	Flexion/Extension
Shoulder	Adduction/Abduction	Internal/External Rotation	Flexion/Extension
Elbow	Adduction/Abduction	Internal/External Rotation	Flexion/Extension

The linear CoM accelerations were calculated by numerically differentiating the CoM position data using the center difference formula for use in the inverse dynamics analysis. The segment angular velocities and accelerations in the anatomical reference frames were also calculated as described in Appendix C.

6.2 Kinematic Analysis for 2D Model

For the 2D model, the global marker positions were projected onto the sagittal plane (only the x and z data was used). Segment angles were calculated using equation (10) and the position data for the two endpoints of each segment:

$$\theta_{segment} = \text{atan}\left(\frac{z_{i+1}-z_i}{x_{i+1}-x_i}\right) \tag{10}$$

where (x_i, z_i) are the coordinates of the endpoint closer to the ground along the chain and (x_{i+1}, z_{i+1}) are the coordinates of the endpoint farther from the ground along the chain.

The x and z components of the linear CoM acceleration calculated for the 3D model were used for the 2D model. The 2D segment angular velocities and accelerations were calculated by numerically differentiating the segment angles using center difference formulas.

6.3 Inverse Dynamics for 3D Model

A diagram of the forces and moments on a segment in the 3D model is shown in Figure 4. The inverse dynamics equations for the forces in the 3D model were derived from the general forms:

$$\sum F_x = F_{p_x} + F_{d_x} = ma_x \tag{11}$$

$$\sum F_y = F_{p_y} + F_{d_y} = ma_y \tag{12}$$

$$\sum F_z = F_{p_z} + F_{d_z} - F_W = ma_z \tag{13}$$

where F_{p_x}, F_{p_y}, and F_{p_z} are the components of the proximal joint force, F_{d_x}, F_{d_y}, and F_{d_z} are the components of the distal joint force, F_W is the force on the segment due to gravity, m is the mass of the segment, and a_x, a_y, and a_z are the acceleration components of the segment CoM (Winter, 2009).

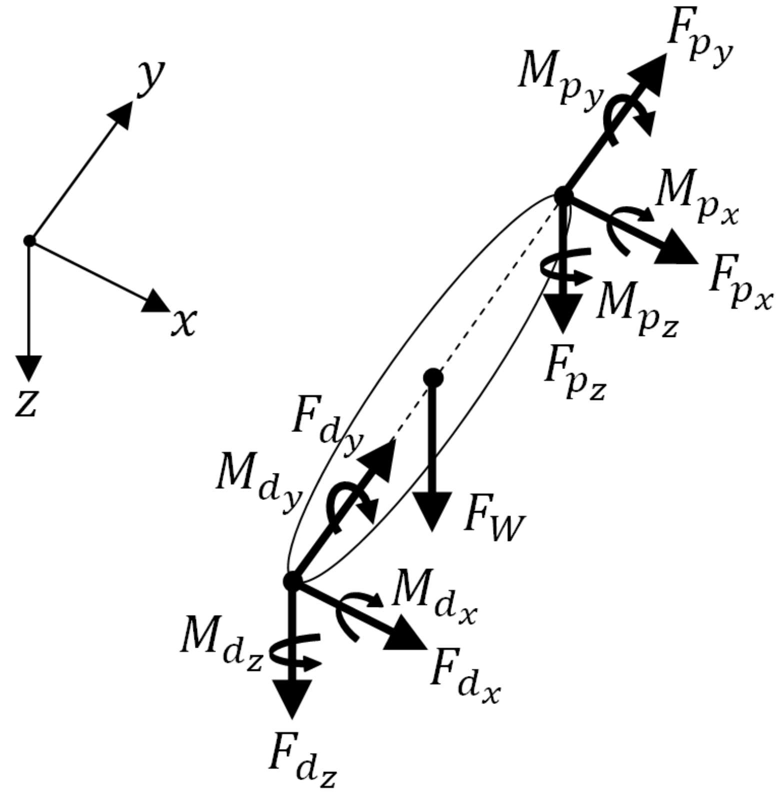

Figure 4: Diagram of Forces and Moments on Segment for 3D Model.

The inverse dynamics equations for the moments in the 3D model were derived from the general form:

$$\sum \vec{M}_G = \vec{M}_d + \left(\vec{l}_d \times \vec{F}_d\right) + \vec{M}_p + \left(\vec{l}_p \times \vec{F}_p\right) = \begin{Bmatrix} I_x\alpha_x + \left(I_z - I_y\right)\omega_y\omega_z \\ I_y\alpha_y + (I_x - I_z)\omega_z\omega_x \\ I_z\alpha_z + \left(I_y - I_x\right)\omega_x\omega_y \end{Bmatrix} \tag{14}$$

where $\vec{F}_d$ is the distal joint force, $\vec{F}_p$ is the proximal joint force, $\vec{M}_d$ is the distal joint moment, $\vec{M}_p$ is the proximal joint moment, $\vec{l}_d$ is the vector from the segment CoM to the distal endpoint, $\vec{l}_p$ is the vector from the segment CoM to the proximal endpoint, I_x, I_y, and I_z are the moments of inertia of the segment about the x-y-z axes, α_x, α_y, and α_z are the components of the segmental angular acceleration about the x-y-z axes, and ω_x, ω_y, and ω_z are the components of the segmental angular velocity about the x-y-z axes (Winter, 2009).

There were six equations for each segment, resulting in 72 equations and 66 unknowns. This is an over-determined system that was solved by determining the reaction forces and moments using both “bottom up” and “top down” inverse dynamics calculations. The lower part of the model was solved from the ground up to the lower back through both lower limbs. The upper part of the model was solved from each hand “down” to the shoulder. Thus, the indeterminacy was resolved by not using the six equations of motion from the trunk segment in the analysis. Vlietstra et al. (2014) found that error increases after crossing the trunk and that this method resulted in good agreement with a solution that solved all the equations in a least squares sense.

With all of the forces in the global reference frame, equations (11) through (13) were solved for each segment to find the proximal reaction forces. For each segment, the proximal and distal joint forces and the distal joint moments were transformed into the anatomical reference frame. Equation (14) was then used to solve for the proximal joint moments. Between segments, the proximal joint moment was transformed to the global reference frame, the sign was flipped to apply it to the segment on the other side of the joint, and then it was transformed to the anatomical reference frame of the next segment where it became the distal joint moment for that segment. The signs on the forces were also flipped between segments.

6.4 Inverse Dynamics for 2D Model

For the 2D case, the forces in the x and z directions on both plates were summed to determine the total ground reaction forces for both feet. The x components of the centers of pressure (COP) for both feet were averaged to determine the overall COP location in the x (fore-aft) direction. The COP location in the z (vertical) direction was set to zero as the subject was applying force to the top surface of the plate throughout the takeoff phase of each jump. A free body diagram was created for each segment with reaction forces and net muscle moments at each joint, as shown in Figure 5.

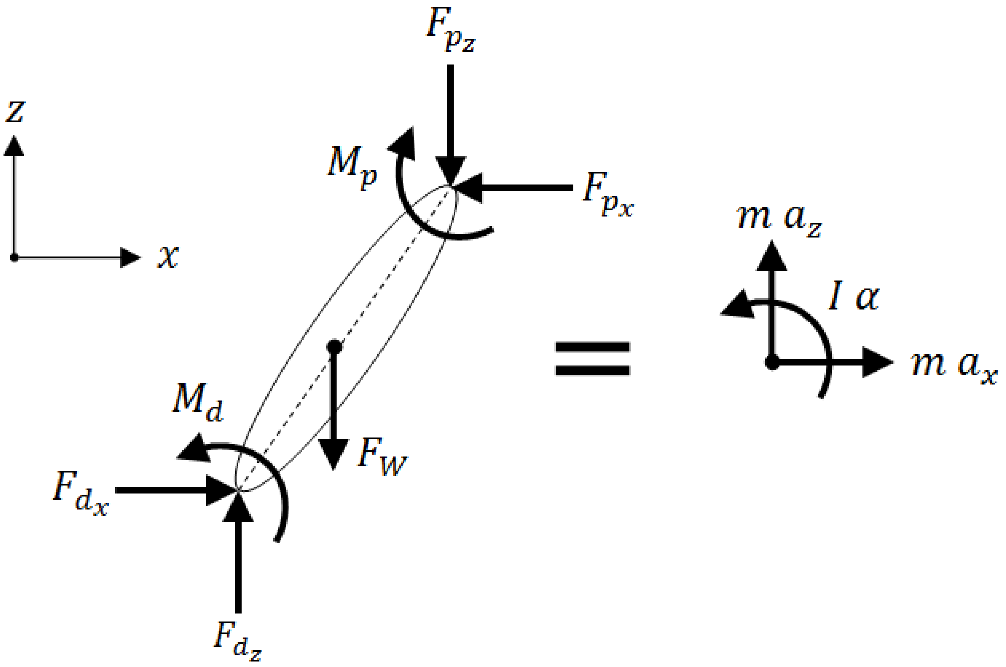

Figure 5: Free Body Diagram for Segment in 2D Model.

Three equations were defined for each segment by applying Newton's 2nd Law and summing the forces and moments as shown in the following equations:

$$\sum F_x = F_{p_x} - F_{d_x} = ma_x \tag{15}$$

$$\sum F_z = F_{p_z} - F_{d_z} - F_W = ma_z \tag{16}$$

$$\sum M = M_p - M_d = I\alpha \tag{17}$$

where F_{p_x} and F_{p_z} are the components of the reaction force at the proximal end of the segment, F_{d_x} and F_{d_z} are the components of the reaction force at the distal end of the segment, F_W is the force of gravity on the segment, m is the segment mass, a_x and a_z are the acceleration components of the segment CoM, M_p is the moment at the proximal end of the segment, M_d is the moment at the distal end of the segment, I is the moment of inertia of the segment in the sagittal plane, and α is the angular acceleration of the segment in the sagittal plane (Winter, 2009).

Equations (15) through (17) were applied to each segment with the forces and moments in the global reference frame. The 2D case also resulted in an over-determined system that was solved by discarding the three equations of motion from the trunk segment. The model was solved from the ground up to the lower back and from the hand "down" to the shoulder.

6.5 Joint Power and Work

To determine the power (P_{joint}) at each joint for the 2D model, the angular velocity of the segment further along the chain from the feet (ω_{i+1}) was subtracted from the angular velocity of the segment earlier in the chain (ω_i) and then multiplied by the joint reaction moment (M_{joint}) as shown below (Winter, 2009).

$$P_{joint} = M_{joint}(\omega_i - \omega_{i+1}) \tag{18}$$

To determine the net power at each joint for the 3D model, the power generated or absorbed at the distal joint (P_d) was added to the power generated or absorbed at the proximal joint (P_p) as shown in equation (19).

$$P_{joint} = P_d + P_p \tag{19}$$

The powers at the distal and proximal joints were calculated using equations (20) and (21) along with the components of the moments ($\vec{M}_d$ and $\vec{M}_p$) and angular velocities ($\vec{\omega}_d$ and $\vec{\omega}_p$) in the segment anatomical reference frames (Winter, 2009).

$$P_d = \vec{M}_d \cdot \vec{\omega}_d = M_{d_x}\omega_{d_x} + M_{d_y}\omega_{d_y} + M_{d_z}\omega_{d_z} \tag{20}$$

$$P_p = \vec{M}_p \cdot \vec{\omega}_p = M_{p_x}\omega_{p_x} + M_{p_y}\omega_{p_y} + M_{p_z}\omega_{p_z} \tag{21}$$

The net work at each joint during the takeoff phase was calculated by numerically integrating the joint power over the 1.2 seconds prior to takeoff.

6.6 Statistics Model

A one-way ANOVA model was used to determine the significance between the results from the 2D and 3D analyses in SAS JMP 10.0 (SAS Institute, Cary, NC, USA). In each analysis, subject was used as a blocking variable in order to compare the difference between the methods while eliminating the effect of the differences between the subjects. The resulting means are plotted along with 95% confidence intervals. For the net work at each joint, the means were also compared using p-values from a Tukey HSD test.

7 Results

The 2D and 3D joint angular velocities for the right side of the body are compared in Figure 6. The 3D angular velocities are those about the z axes of the anatomical reference frames. Positive angular velocity in the plots corresponds to extension of the joint (increasing joint angle). No significant difference can be seen between the angular velocities for the 2D and 3D analyses of the joints in the lower body. However, a significant difference can be seen between the angular velocities for the shoulder and the elbow.

The net joint moments from the 2D and 3D analyses for the right side of the body are compared in Figure 7. The 3D moments shown in the plot are those about the z axes of the anatomical reference frames (corresponding to the flexion/extension moment) and are shown in the anatomical reference frame of the distal segment. Extension (and plantarflexion) moments are positive in the plots.

At the beginning of the jump cycle in Figure 7, the moment at each joint was small and then started to increase rapidly 0.8 to 0.6 seconds before takeoff, reaching a peak extension moment 0.4 to 0.1 seconds before takeoff. Very little significant difference is seen between the moments about the z-axis (flexion/extension) for the 2D and 3D analyses at each joint with the exception of the shoulder. For the shoulder, the 2D and 3D methods were in agreement until 0.4 seconds before the jump. At this point, the two curves separated with the 2D method staying in extension longer and then reaching a larger flexion moment before takeoff. The 2D and 3D methods were in agreement for the knee, hip, and lower back throughout the full jump cycle.

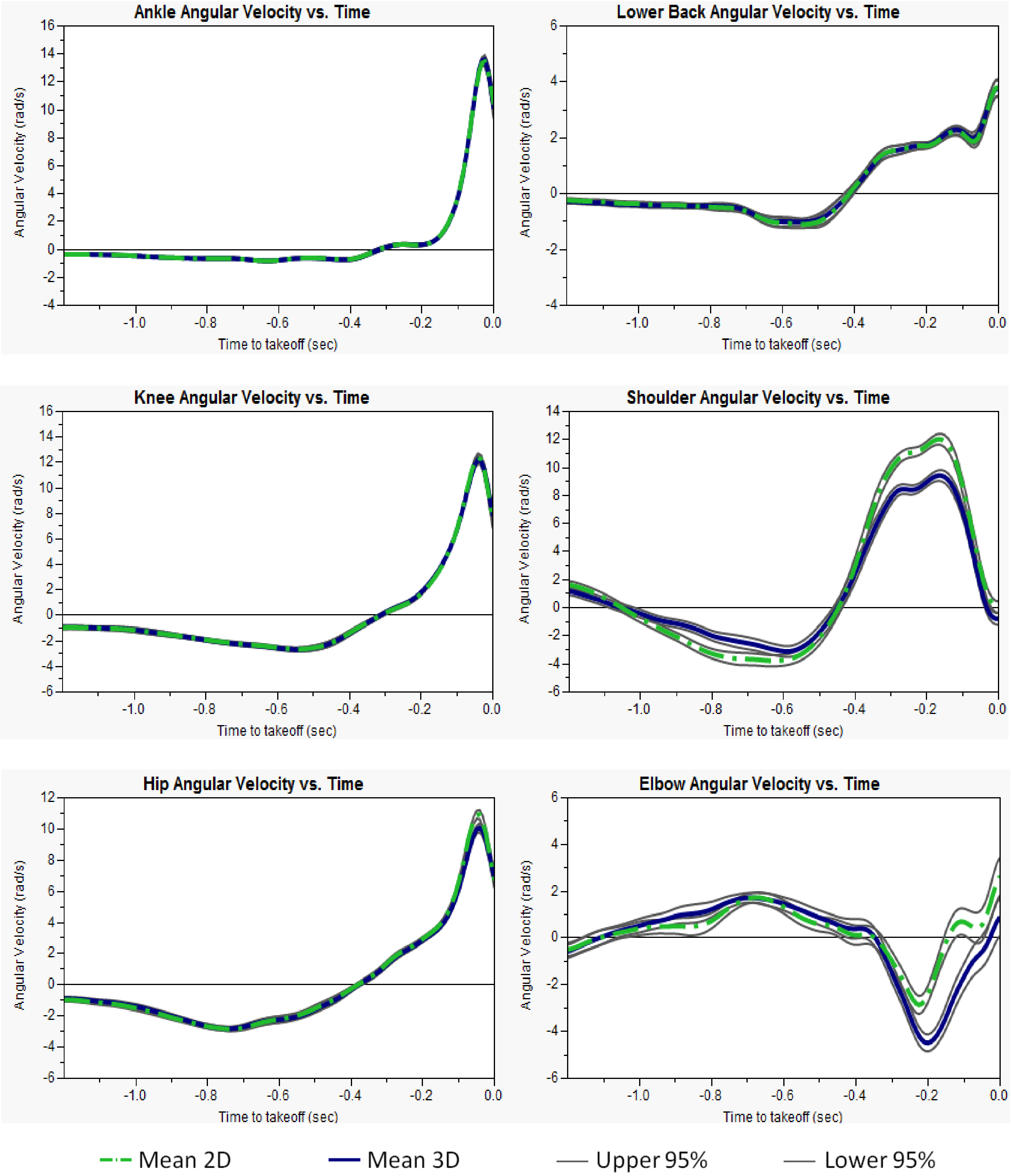

Figure 6: Comparison of Joint Angular Velocity for 2D and 3D Analyses (Right Side).

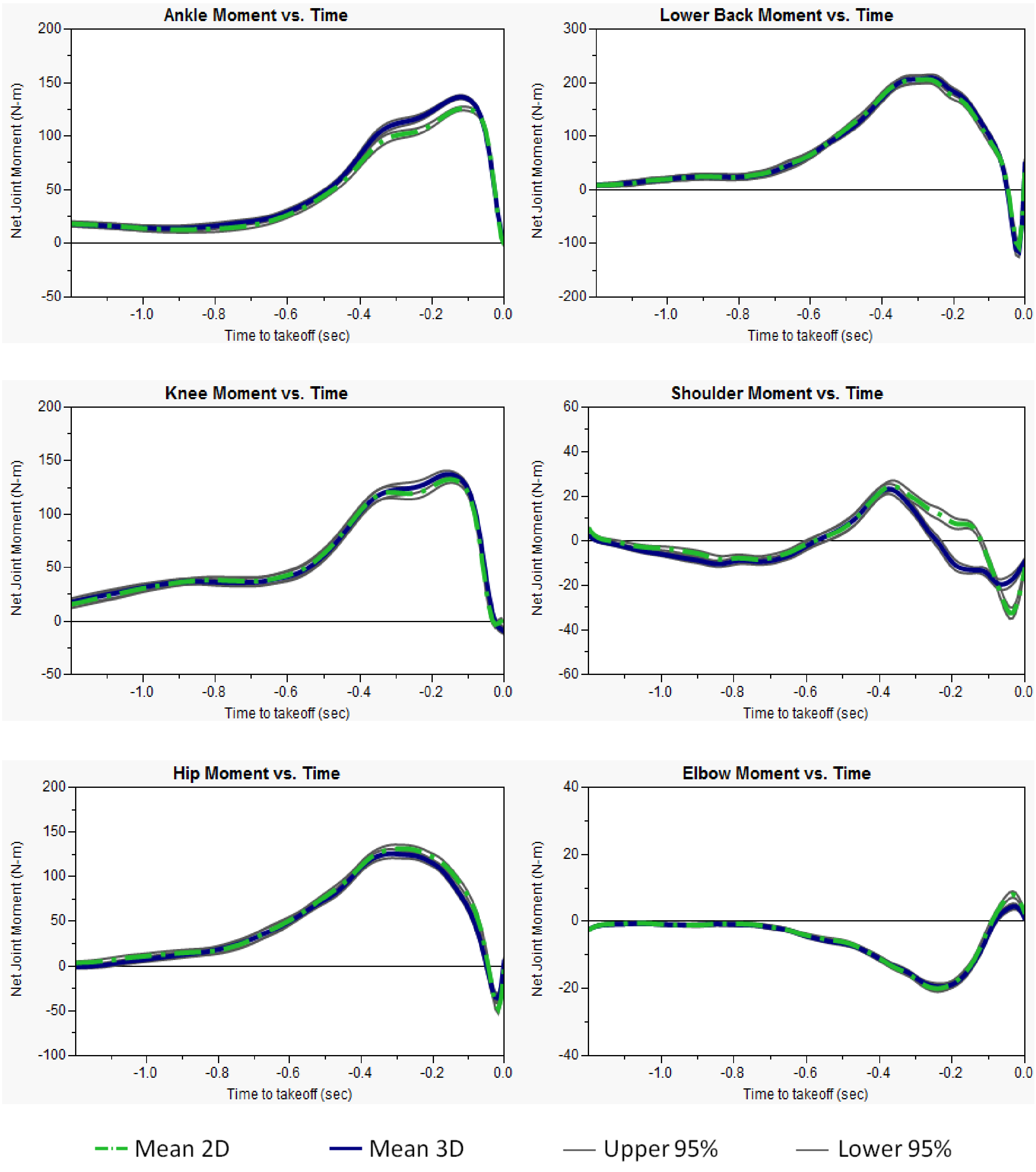

Figure 7: Comparison of Net Flexion/Extension Moments at Each Joint for 2D and 3D Analyses (Right Side).

In the ankle plot in Figure 7, the methods were in agreement at the beginning and end of the cycle but the confidence intervals do not overlap as the moment increased to peak plantarflexion with the 3D moment being slightly larger than the 2D moment. In the elbow plot, the methods were in agreement until 0.1 seconds before takeoff where the 2D analysis resulted in a slightly higher extension moment.

Figure 8 shows the moments about the x, y, and z axes for the 3D analysis in the anatomic reference frames of the distal segments. The sign conventions for the plots are given in Table 5 (abduction, external rotation, and extension are positive). For most of the joints, the moment about the z-axis was much larger than the moments about the other axes, indicating that the primary moment was flexion/extension. However, significant moments about the x-axes (adduction/abduction) at the hip and shoulder are also seen in the figure. At the hip, the moment about the x-axis was very small for the beginning of the jump cycle and then increased to a peak abduction moment at about 0.1 seconds before takeoff. At the shoulder, the moment about the x-axis also started near zero, increasing to a peak abduction moment about 0.2 seconds before takeoff and then reaching a smaller peak adduction moment less than 0.1 seconds before takeoff.

This result at the shoulder coincided with the visual observations made throughout the data collection process. Shoulder abduction and adduction was physically observed during the standing long jump motion for all of the subjects. Figure 9 also demonstrates the existence of out-of-plane motion in the upper body. These graphs show the distance from the shoulder joint center to the elbow and wrist joint centers along the y-axis of the lab coordinate system. Motion in the lateral direction (away from the center of the body) is shown as positive on the plots.

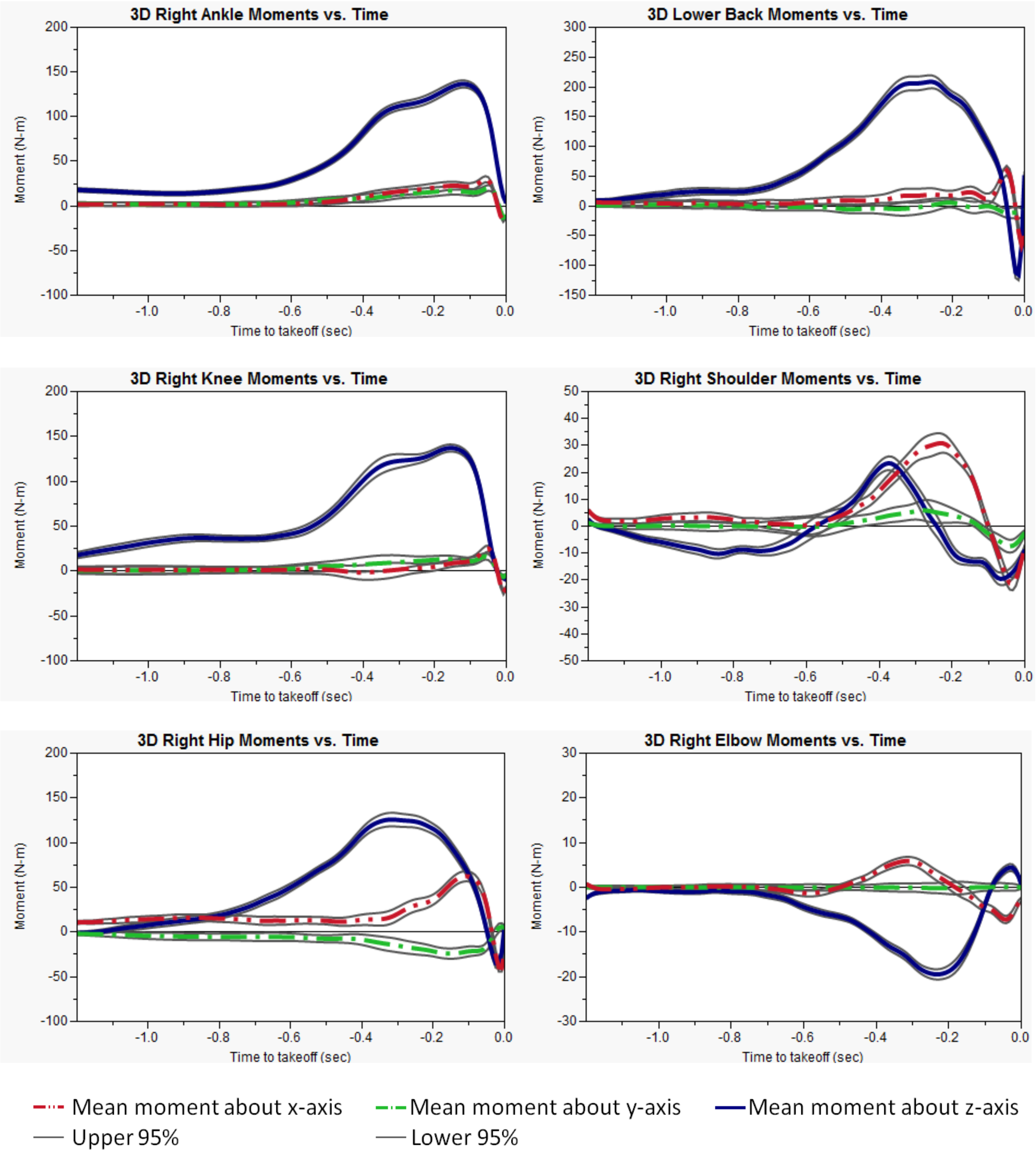

Figure 8: Mean Components of Joint Moments for the 3D Analysis (Right Side).

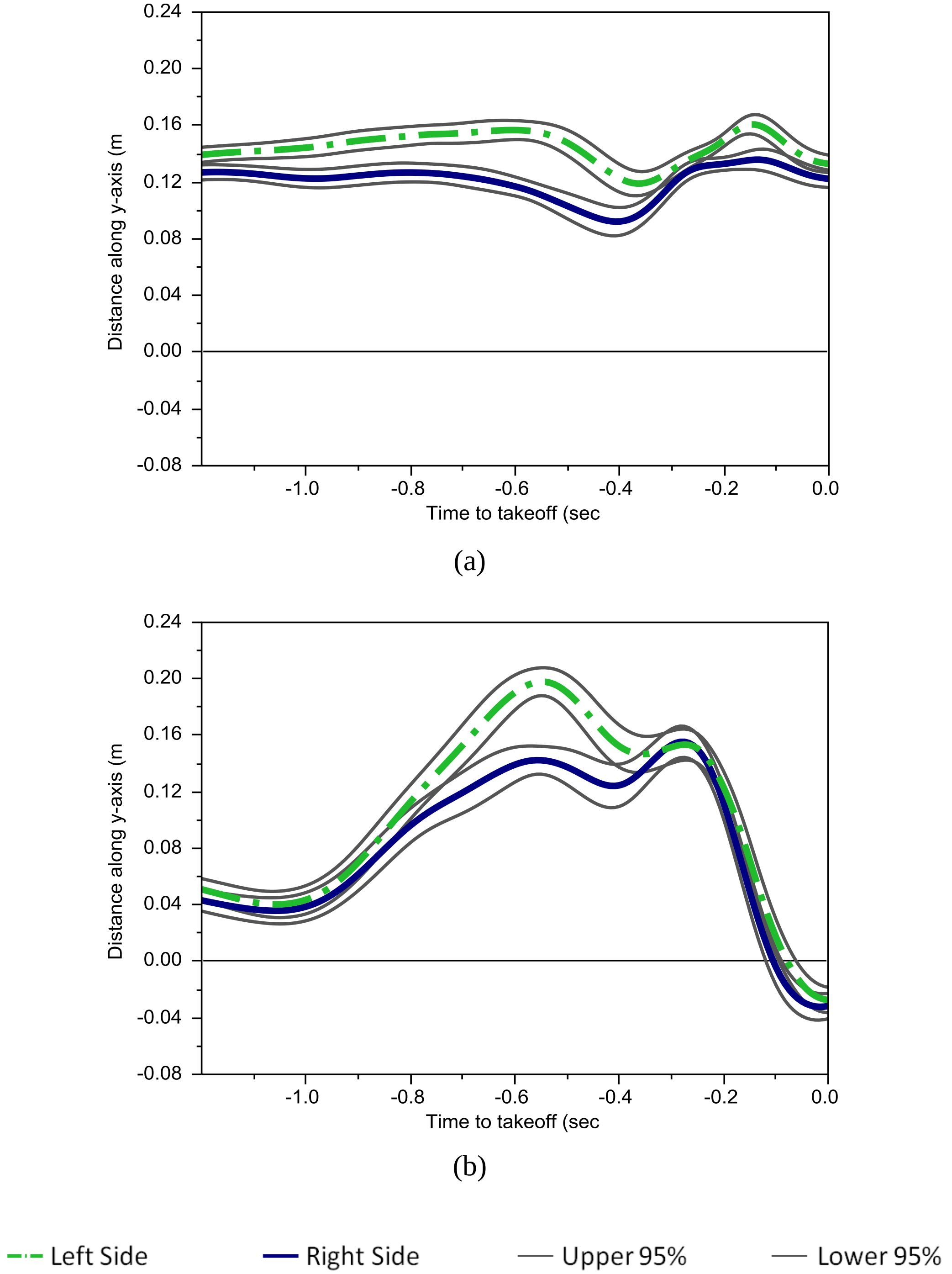

(a)

(b)

Figure 9: Mean Lateral Positions of (a) Elbow Joint Centers and (b) Wrist Joint Center Relatives to Shoulder Joint Centers.

Figures 10 and 11 show the power results from the jumping study. In Figure 10, the power generated (positive) or absorbed (negative) at each joint for both methods are shown with the 3D power being the power about the z-axis. There was very little difference between the methods for the four joints in the lower body (ankle, knee, hip, and lower back). For the hip, there was good agreement for most of the jump but the confidence intervals did not overlap at peak power generation, with the 2D analysis reaching a higher peak power. For the elbow and shoulder, there were significant differences between the power results from the two methods. There was good agreement between the methods for both joints until 0.4 seconds before takeoff. At this point, the 2D method at the shoulder resulted in a higher peak power generation and stayed in power generation longer. The 3D method resulted in more power absorption for the shoulder in comparison to the 2D method. For the elbow, the 3D method resulted in a peak power generation twice as high as the 2D method.

In Figure 11, the x, y, and z components of power from the 3D analysis are shown. Most of the power at the joints was generated about the z-axis (due to the flexion/extension motion). The hip also showed some power generation about the x-axis (due to adduction/abduction). The shoulder appears to be the only joint that was not dominated by the flexion/extension motion as significant power generation and absorption was shown about both the x and z axes at the shoulder. The plot shows that peak power generation actually occurred about the x-axis. The powers about the two axes acted in the opposite directions, with the x-axis reaching peak power generation as the z-axis reached peak power absorption (at 0.2 seconds before takeoff).

Figures 10 and 11 also show that the confidence intervals are larger at the shoulder and elbow than at the other joints prior to takeoff, indicating greater variability between jumps and subjects in the upper body.

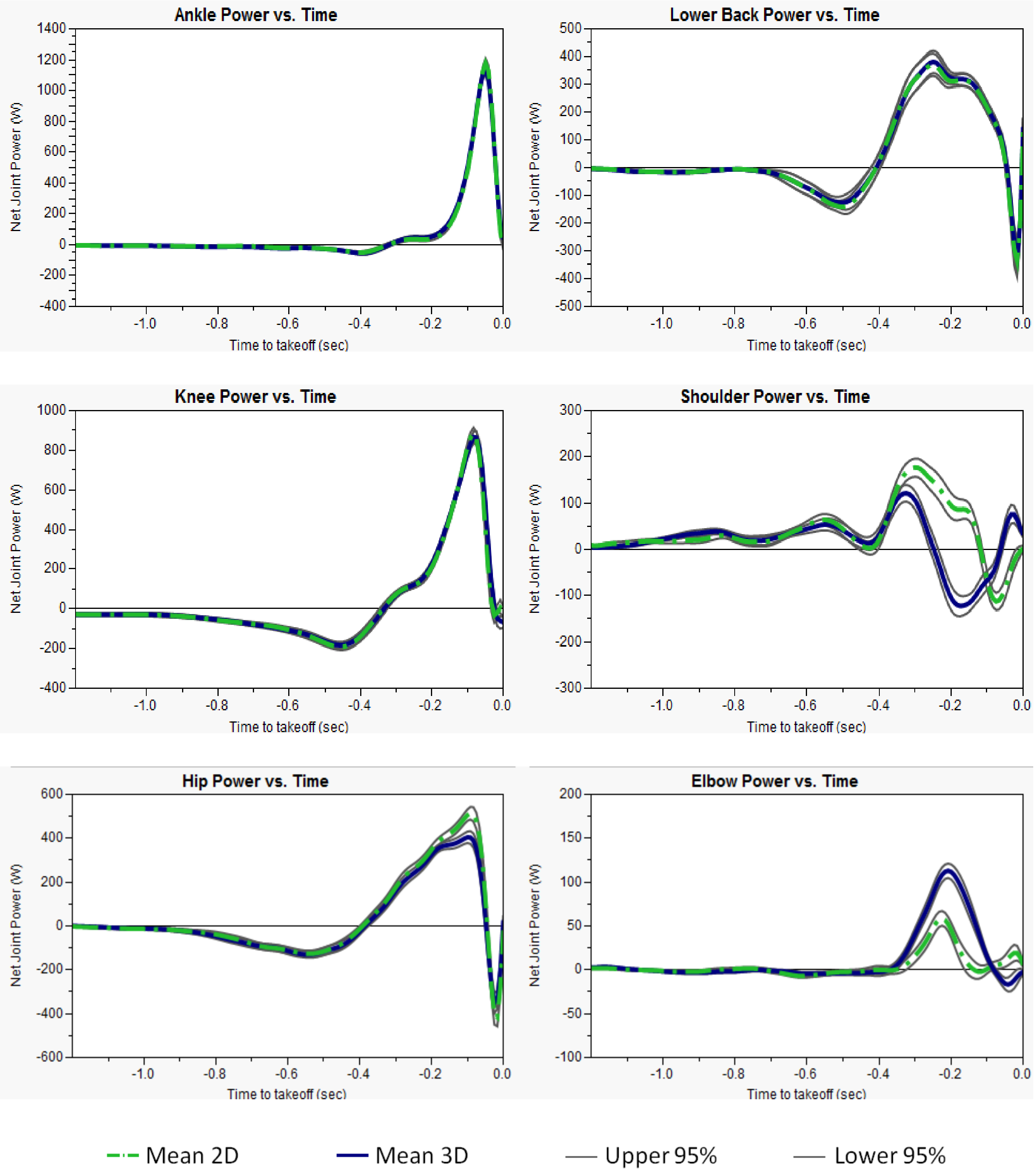

Figure 10: Comparison of Net Joint Power for 2D and 3D Analyses (Right Side).

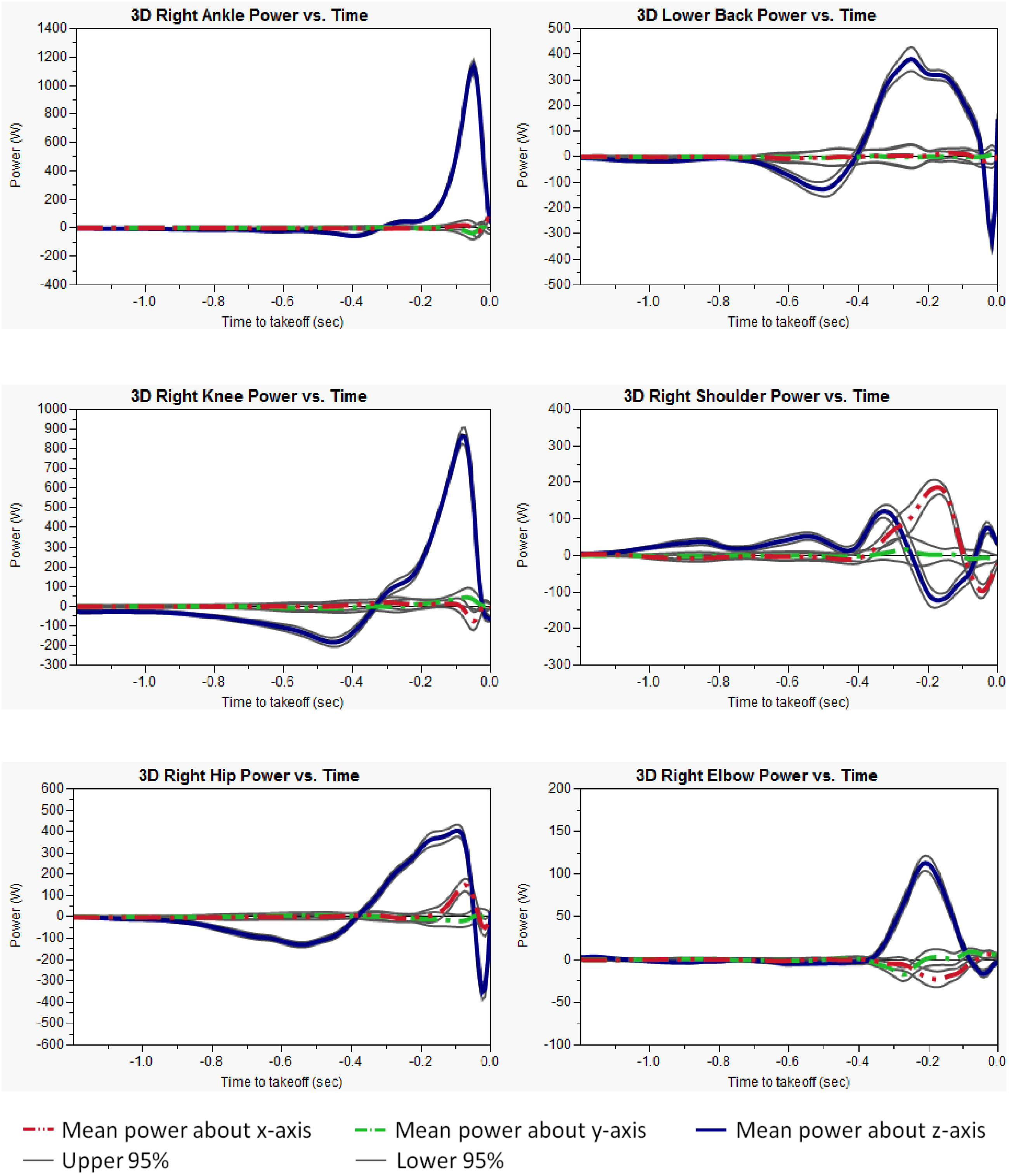

Figure 11: Mean Components of Power for the 3D Analysis (Right Side).

The work for the 3D case was the sum of the work performed about all three components of the anatomical reference frame for each joint. Figure 12 shows the net work performed at each joint (with means and 95% confidence intervals from a one-way ANOVA analysis) for both the 2D and 3D methods on the left and right sides of the body. Methods 1 and 2 in this plot correspond to the 2D work resulting from using the markers on the left and right sides of the body, respectively. Methods 3 and 4 correspond to the 3D work for the joints on the left and right sides of the body.

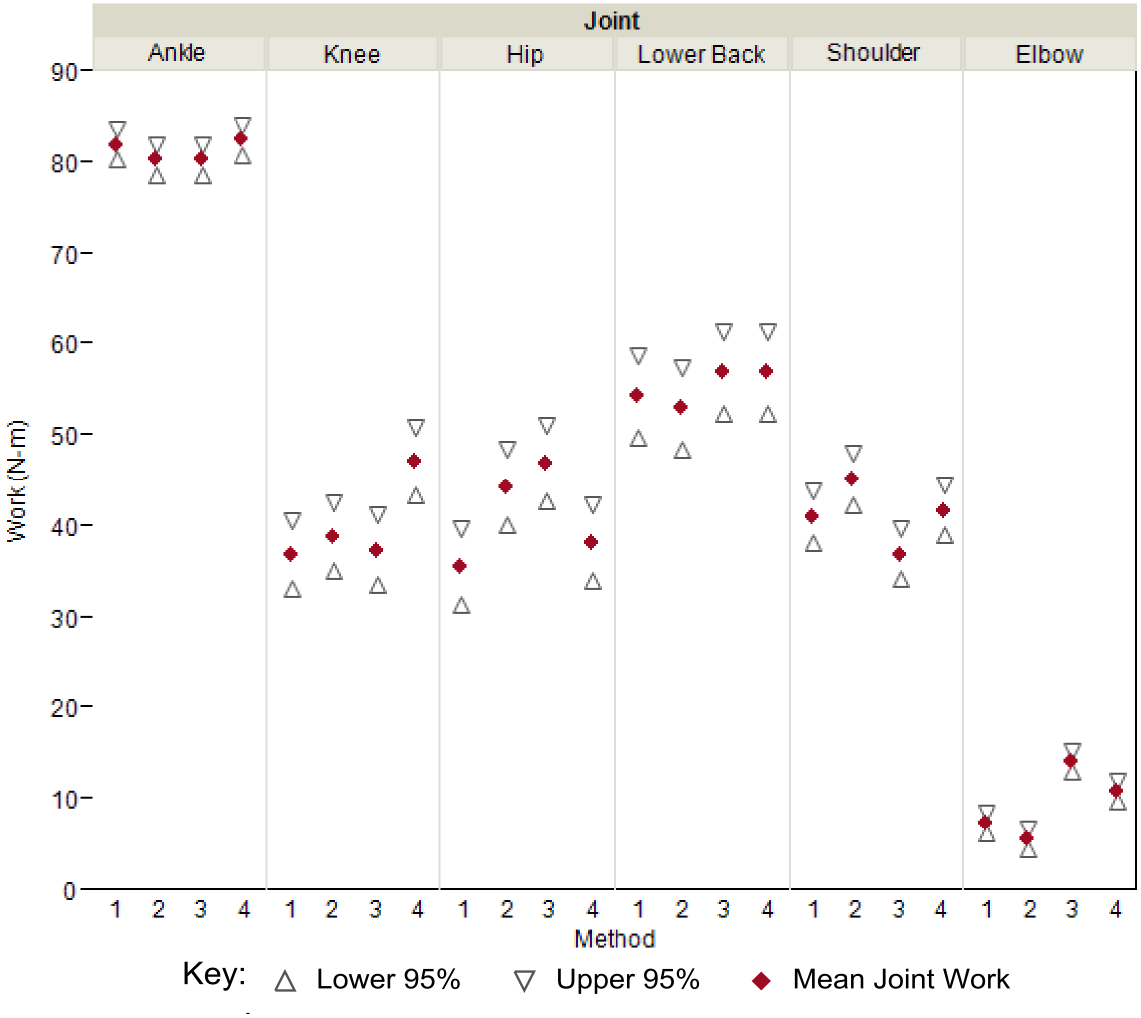

Figure 12: Mean Net Joint Work Comparison (Method 1: 2D left side, Method 2: 2D right side, Method 3: 3D left side, Method 4: 3D right side).

For the 3D analysis in Figure 12, the work at the lower back joint was the exact same for both the left and right sides as there was only one lower back joint in the 3D model. There was positive work at all of the joints, with the largest amount of work being performed by the ankle. Between the methods, there was good agreement and very little significant difference can be seen. There were significant differences at both elbows, with the total work from the 3D method slightly higher than the work from the 2D method. The confidence intervals also seem to be separate for the work from the 2D and 3D methods at the left hip and right knee.

After the one-way ANOVA was performed, a Tukey HSD test was run on the work results for a post-hoc analysis. Table 6 shows the resulting p-values for comparisons between the mean net work from the 2D and 3D methods for both sides of the body. P-values that indicate a significant difference ($p < 0.05$) are bolded. This table confirms that the differences between the two methods for the elbows, the left hip, and the right knee were significant. The p-values for the elbows are both less than 0.0001, indicating a very significant difference.

Table 6: P-Values for Comparison of Mean Net Joint Work from 2D and 3D Models.

Joint	**2D Work vs. 3D Total Work**	
	Left (1 vs. 3)	**Right (2 vs. 4)**
Ankle	0.7311	0.4492
Knee	1.0000	**0.0251**
Hip	**0.0020**	0.3069
Lower Back	0.9659	0.8328
Shoulder	0.3524	0.5738
Elbow	**<0.0001**	**<0.0001**

Further results from the Tukey HSD test are shown in Table 7 with p-values for comparisons between the left and right sides of the body for the 2D and 3D work. A larger number of joints showed significant differences between the work performed by the left and right sides when using a 3D analysis. For the 3D method, the knee, hip, and elbow showed a significant difference between the sides while for the 2D method, the hip is the only joint that showed a significant difference.

Table 7: P-Values for Comparison of Mean Net Joint Work for Left and Right Sides.

Joint	**Left vs. Right Solution Pair**	
	2D Work	3D Work
Ankle	0.7327	0.4475
Knee	0.9800	**0.0046**
Hip	**0.0389**	**0.0379**
Lower Back	0.9987	1.0000
Shoulder	0.3397	0.1750
Elbow	0.2432	**0.0008**

Whereas Figure 12 and Table 6 show that the total 3D work at the shoulder was not significantly different from the 2D work, earlier results for the 3D components of moment and power at the shoulder in Figures 8 and 11 indicate that the out-of-plane motion at this joint was significant. The x components of the moments and power were on the same order of magnitude as the z components of the moments and power. To investigate the effect of the different components on the total work, the 3D shoulder work was separated into the work performed about different axes. The x and y components of work at the other joints were zero or near zero. The percentages (based on mean values) of total shoulder work due to the different components from the 3D method are shown in Table 8 for the left and rights sides of the body. Table 8 shows that the total work at the shoulder was split between work about the x-axis (adduction/abduction) and work about the z-axis (flexion/extension). Approximately 50% of the work at the joint is due to each of these components. Less than 3% of the work is due to the y component (internal/external rotation). A significant difference was also seen between the left and right sides, with a larger x component of the work on left side and a larger z component of the work on the right side. This indicates a lack of symmetry between the sides of the body.

Table 8: Percentage of Shoulder Work Due to Different Components in 3D Analysis.

Component	**Left**	**Right**
About x-axis	50.58%	45.29%
About y-axis	2.89%	1.13%
About z-axis	46.53%	53.58%

8 Discussion

The results from this study show good agreement between the 2D and 3D methods for the lower body. There was very little difference in the angular velocities (Figure 6), moments (Figure 7), power (Figure 10), and work (Figure 12) for the ankle, knee, hip, and lower back. The plots from the 3D analysis in Figures 8 and 11 show that the moment and power about the z-axis (flexion/extension) were dominant for these joints and there was little moment or power that was not about this axis. This indicates that in the lower body for the standing long jump, there is mostly planar motion that is well approximated by the 2D model. The hip was the only joint in the lower body that showed significant moments (Figure 8) and power generation (Figure 11) about another axis (the x-axis). This was expected as the hip is a ball joint that is not physically constrained to planar motion and has more degrees of freedom. While the moments and power about the z-axis from the 3D analysis agree well with the 2D analysis, the planar assumption did cause the effects of the adduction/abduction moment to be lost at this joint. However, flexion/extension was still the dominant motion at the hip and there was no significant difference between the 2D work and the total 3D work resulting from these analyses.

Significant differences between the methods began to be noticed in the analysis of the upper body. This was expected as more out-of-plane motion occurs in the upper body than in the lower body during the standing long jump. The upper body out-of-plane motion in this study is shown by the mean positions of the elbow and wrist joint centers relative to the shoulder joint centers in Figure 9. There was still fairly good agreement between the moments at the elbow and the work at the shoulder for the two methods. The small difference in moments at the elbow is likely due to the projection of the 3D positions onto the sagittal plane for the 2D analysis, which changed the flexion/extension angle at the elbow. However, significant differences in the moment at the shoulder and in the power generation at both the elbow and shoulder are seen in Figures 7 and 10, respectively. Significant moments and power generation are also seen in more than one component (about both the x and z axes) at the shoulder joint in Figures 8 and 11. As shown in Figure 12 and Table 6, the elbow was one of the only joints with a significant difference between the work resulting from the 2D and 3D methods.

There were larger differences in the power generation than in the moments for the upper body. Since power is the combination of the joint moment and angular velocity, the angular velocity is what caused the difference in power when the moments were similar. This can be seen by comparing the 2D and 3D angular velocity (Figure 6), moment (Figure 7), and power (Figure 10) plots. At the shoulder, the angular velocity and moment from the 2D analysis both had a slightly higher peak before takeoff. Therefore, the power plot shows a large difference between the 2D and 3D analyses when these two smaller differences are multiplied together. At the elbow, there was very little difference between the 2D and 3D analyses in the moment plot. In the angular velocity plot, the flexion peak from the 3D analysis was larger (more negative) than the flexion peak from the 2D analysis. This difference in angular velocity caused the power generation peak for the 3D analysis to be much larger than for the 2D analysis even though the moments were the same.

The shapes of the moment curves (Figure 7) and power curves (Figure 10) were similar for all of the joints except the elbow. This was also due to the angular velocities (Figure 6). The shoulder angular velocities and moments both show a positive peak (due to extension of the joint) at 0.2 to 0.4 seconds before takeoff. Multiplying these angular velocities and moments resulted in a high positive (power generation) peak before takeoff as both the angular velocity and moment were in the same direction (extension). The elbow angular velocities and moments both reached a negative peak (due to flexion of the joint) at about 0.2 seconds before takeoff. The angular velocities and moments were in the same direction (flexion) so multiplying them together also resulted in a positive power generation peak before takeoff.

This study shows that there were significant differences in the upper body results from the two models, particularly with respect to power generation. The 2D model could not represent the out-of-plane motion that occurred in the upper body as the adduction/abduction motion at the shoulder was ignored and the elbow angles were projected onto the sagittal plane. Separating the work into components at the shoulder (Table 8) showed that an approximately equal amount of work was performed about the x and z axes during the standing long jump. In the 2D model, it was assumed that all of the work was performed in the sagittal plane (all flexion/extension work). If this distinction is important, a 3D analysis would be required. However, the overall work resulting from both methods was the same so if a study is only concerned about the total work at the joints, a 2D model would likely be sufficient.

The comparison between the results from the left and right sides of the body in Table 7 indicate a lack of symmetry that may be lost with an analysis that assumes sagittal plane motion and bilateral symmetry. The fairly large differences between the sides in percentage of shoulder work due to the x and z components (Table 8) support this lack of symmetry. The 2D model may not capture significant differences between the two sides that can be seen with a 3D model. The assumption of sagittal plane motion does not allow for differences in out-of-plane motion between the two sides of the body. A 3D model may be only way to capture asymmetry details of jumping in elite athletes, where it may be vital. The lack of symmetry in this sample also suggests that jumping study results may differ based on what side of the body is used during a

2D analysis. This comparison indicates that further work should be done investigating the assumption of bilateral symmetry.

Another area of further work is upper body modeling and analysis. The larger confidence intervals for the elbow and shoulder indicate greater variability in the upper body during the standing long jump. There was also less confidence in the results of this study for the upper body. This was partially due to significant noise in the linear and angular accelerations, which had a larger effect in the upper body where the accelerations were larger and the masses of the segments were smaller. This variability may be reduced by using a different filtering method, possibly by spline fitting the motion capture data instead of using a Butterworth filter. Cross-talk, in which the axes of the anatomical reference frames defined by the markers are not aligned with the physiological axes of rotation, at the shoulder and elbow may have also affected the results. The actual motion at the joints in the upper body may not have been accurately represented by the moments about the anatomical axes as presented in this study. Improved marker placement and coordinate system definition should be investigated to increase the accuracy of the 3D model for the upper body.

The main limitation of this study is that the models used have not been fully validated or tested for reliability. The 3D model was based on commonly used reference frames and inertial parameters; however adaptations were made for this study. Prior to future studies, the 2D and 3D models should be validated by comparing gait and jumping results to published data. Another limitation is the small sample size used for this study. With only six subjects, the results are not able to be generalized to an entire population. The subjects in this study showed asymmetry between the left and right sides during jumping but these results do not represent other samples. Data should be collected on a greater number of subjects in order to make further conclusions about the single plane and symmetry assumptions in jumping.

9 Conclusion

The standing long jump is generally considered to be a planar motion and in most studies the assumption of planar motion is built into the data collection and analysis. In this study, this assumption was investigated by collecting 3D data and analyzing it both with and without the assumption of planar motion. Motion capture data and ground reaction forces were collected for the takeoff phase of the standing long jump. The cycle for the jump was considered to start 1.2 seconds before takeoff, where takeoff was defined as the moment in which both feet left the ground and the ground reaction forces went to zero. These data were analyzed using both a 2D and a 3D model of the body. Inverse dynamics analyses were then performed to determine the joint moments, power, and work. A one-way ANOVA analysis was used to compare the results of the two models. This study found that there is generally good agreement between 2D and 3D models for lower body while significant differences exist between the models for the upper body, particularly in power generation. However, the work performed at all of the joints was found to be very similar from both models.

When choosing a model for the analysis of the standing long jump, the value added by a 3D model needs to be considered with respect to the goals of the study. The results of this study show that a planar motion assumption should be appropriate and a 2D model should be sufficient for most studies of the standing long jump, particularly when overall performance is considered and details of the upper body motion are not a concern. In cases where upper body motion is being studied or small increases in performances are vital (such as in athletic training), a 3D model may be more appropriate as it more accurately represents the motion of the upper body and is better able to show the differences in performance between the two sides of the body.

10 References

Aguado, X., Izquierdo, M., Montesinos, J.L., 1997. Kinematic and kinetic factors related to the standing long jump performance. Journal of Human Movement Studies 32, 156-169.

Anderson, F.C., Pandy, M.G., 1999. A dynamic optimization solution for vertical jumping in three dimensions, Computer Methods in Biomechanics and Biomedical Engineering 2, 201–231.

Ashby, B., Heegaard, J.H., 2002. Role of arm motion in the standing long jump. Journal of Biomechanics 35, 1631-1637.

Begon, M., Monnet, T., Lacouture, P., 2007. Effects of movement for estimating the hip joint centre. Gait & Posture 25, 335-359.

Camomilla, V., Cereatti, A., Vannozzi, G., Cappozzo, A., 2006. An optimized protocol for hip joint centre determination using the functional method. Journal of Biomechanics 39, 1096-1106.

Cappozzo, A., 1984. Gait analysis methodology. Human Movement Science 3, 27–50.

Cappozzo, A., Catani, F., Della Cruce, U., Leardini, A., 1995. Position and orientation of bones during movement: anatomical frame definition and determination. Clinical Biomechanics 10, 171-178.

Cereatti, A., Donati, M., Camomilla, V., Margheritini, F., Cappozzo, A., 2009. Hip joint centre localization: An ex vivo study. Journal of Biomechanics 42, 818-823.

Clancy, K., 2010. Comparison of lumbar spine loads during back and front squats (Master's thesis). State University of New York College at Cortland, Cortland, NY.

Davis, R.B., Ounpuu, S., Tyburski, D., Gage, J.R., 1991. A gait analysis data collection and reduction technique. Human Movement Science 10, 575-587.

de Leva, P., 1996. Adjustments to Zatsiorsky-Seluyanov's segment inertia parameters. Journal of Biomechanics 29, 1223-1230.

Delonge, P., 1972. Computer optimization of Deschamp's method and error cancellation in reflectometry. In: Proceedings of the IMEKO Symposium on Microwave Measurement, Budapest.

Ehrig, R.M., Taylor, W.R., Duda, G.N., Heller, M.O., 2006. A survey of formal methods for determining the centre of rotation of ball joints. Journal of Biomechanics 39, 2798-2809.

Filush, A., 2012. Effect of using hand-weights on performance in the standing long jump (Master's thesis). Grand Valley State University, Allendale, MI.

Gamage, S.S.H.U. and Lasenby, J., 2002. New least squares solutions for estimating the average centre of rotation and the axis of rotation. Journal of Biomechanics 35, 97-93.

Halvorsen, K., 2003. Bias compensated least squares estimate of the center of rotation. Journal of Biomechanics 36, 999-1008.

Harrington, M.E., Zavatsky, A.B., Lawson, S.E.M., Yuan, Z., Theologis, T.N., 2007. Prediction of the hip joint centre in adults, children, and patients with cerebral palsy based on magnetic resonance imaging. Journal of Biomechanics 40, 595-602.

Hay, J.G., Miller, J.A., Canterna, R.W., 1986. The techniques of elite male long jumpers. Journal of Biomechanics 19, 855-866.

Holzreiter, S., 1991. Calculation of the instantaneous centre of rotation for a rigid body. Journal of Biomechanics 24, 643–647.

Kasa, I., 1976. A circle fitting procedure and its error analysis. IEEE Transactions on Instrumentation and Measurement 25, 8–14.

Lariviere, C., Gagnon, D., 1999. The influence of trunk modeling in 3D biomechanical analysis of simple and complex lifting tasks. Clinical Biomechanics 14, 449-461.

Leardini, A., Cappozzo, A., Catani, F., Toksvig-Larsen, S., Petitto, A., Sforza, V., Cassanelli, G., Giannini, S., 1999. Validation of a functional method for the estimation of hip joint centre location. Journal of Biomechanics 32, 99-103.

Lempereur M, Leboeuf F, Brochard S, Rousset J, Burdin V, Rémy-Néris, O., 2010. In vivo estimation of the glenohumeral joint centre by functional methods: accuracy and repeatability assessment. Journal of Biomechanics 43: 370–374.

Lopomo, N., Sun, L., Zaffagnini, S., Giordano, G., Safran, M.R., 2010. Evaluation of formal methods in hip joint center assessment: An in vitro analysis. Clinical Biomechanics 25, 206-212.

Mackala, K., Stodólka, J., Siemienski, A., Coh, M., 2013. Biomechanical analysis of standing long jump from varying positions. Journal of Strength and Conditioning Research 27, 2674–2684.

MacWilliams, B.A., 2008. A comparison of four functional methods to determine centers and axes of rotations. Gait & Posture 28, 673-679.

Marin, F., Mannel, H., Claes, L., Durselen, L., 2003. Accurate determination of a joint centre center based on the minimal amplitude point method. Computer Aided Surgery 8, 30–34.

Monnet, T., Desailly, E., Begon, M., Vallee, C., Lacouture, P., 2007. Comparison of the SCoRE and HA methods for locating in vivo the glenohumeral joint centre. Journal of Biomechanics 40, 3487-3492.

Nikooyan, A.A., van der Helm, F.C.T., Westerhoff, P., Graichen, F., Bergmann, G., Veeger, H.E.J., 2011. Comparison of two methods for in vivo estimation of the glenohumeral joint rotation center (GH-JRC) of the patients with shoulder hemiarthroplasty. PLoS ONE 6, 1-7.

Pandy, M.G., Zajac, F.E., Sim, E., Levine, W.S., 1990. An optimal control model for maximum-height human jumping, Journal of Biomechanics 23, 1185–1198.

Pratt, V.R., 1987. Direct least-squares fitting of algebraic surfaces. Computer Graphics 21, 145-152.

Ren, L., Jones, R.K., Howard, D., 2008. Whole body inverse dynamics over a complete gait cycle based only on measured kinematics. Journal of Biomechanics 41, 2750-2759.

Reynolds, H.M., Snow, C.C., Young, J.W., 1982. Spatial geometry of the human pelvis, Technical report, FAA-AM-82-9, FAA Civil Aeromedical Institute, Oklahoma City, OK.

Sangeux, M., Peters, A., Baker, R., 2011. Hip joint centre localization: Evaluation on normal subjects in the context of gait analysis. Gait & Posture 34, 324-328.

Schwartz, M.H., Rozumalski, A., 2005. A new method for estimating joint parameters from motion data. Journal of Biomechanics 38, 107–116.

Seidel, G.K., Marchinda, D.M., Dijkers, M., Soutas-Little, R.W., 1995. Hip joint center location from palpable bony landmarks – a cadaver study. Journal of Biomechanics 28, 995-998.

Stoddart, A.J., Mrázek, P., Ewins, D., Hynd, D., 1999. A computational method for hip joint centre location from optical markers. In: Proceedings of the BMVC 99, Proceedings of the 10th British Machine Vision Conference. Nottingham, UK.

Vlietstra, N., 2014. Comparing methods for full body inverse dynamics analysis of a standing long jump (Master's thesis). Grand Valley State University, Allendale, MI.

Wakai, M., Linthorne, N.P., 2005. Optimum take-off angle in the standing long jump. Human Movement Science 24, 81-96.

Winter, D., 2009. Biomechanics and motor control of human movement, fourth edition. John Wiley and Sons, Waterloo, Ontario, Canada.

Woltring, H.J., Huiskes, R., de Lange, A., Veldpaus, F.E., 1985. Finite centroid and helical axis estimation from noisy landmark measurements in the study of human joint kinematics. Journal of Biomechanics 18, 379–389.

Wu, G., Siegler, S., Allard, P., Kirtley, C., Leardini, A., Rosenbaum, D., Whittle, M., D'Lima, D.D., Cristofolini, L., Witte, H., Schmid, O., Stokes, I., 2002. ISB recommendation on definitions of joint coordinate systems of various joints for the reporting of human joint motion – part I: ankle, hip, spine. Journal of Biomechanics 35, 543-548.

Wu, G., van der Helm, F.C.T., Veeger, H.E.J., Makhsous, M., Van Roy, P., Anglin, C., Nagels, J., Karduna, A.R., McQuade, K., Wang, X., Werner, F.W., Buchholz, B., 2005. ISB recommendation on definitions of joint coordinate systems of various joints for the reporting of human joint motion – Part II: shoulder, elbow, wrist, hand. Journal of Biomechanics 38, 981-992.

Yoshioka, S., Nagano, A., Hay, D.C., Fukashiro, S., 2010. The effect of bilateral asymmetry of muscle strength on jumping height of the countermovement jump: A computer simulation study. Journal of Sports Sciences 28, 209-218.

Zatsiorsky, V.M., Seluyanov, V.N., Chugunova, L.G., 1990. Methods of determining mass-inertial characteristics of the main segments of the human body. In Biomechanics VIII-B (Edited by Matsui, H. and Kobayashi, K.), Human Kinetic, Illinois, 1152-1159.

11 Appendices

11.1 Appendix A: 3D Kinematic Model

Following are descriptions of the anatomical coordinates systems used in the model (adapted from ISB recommendations). All x-axes point in the anterior direction, all y-axes are along the long axis of the segment and point in the proximal direction, and all z-axes point towards the right side of the subject. Abbreviations used in this summary are consistent with Table 1.

Foot Coordinate System – origin at HEE

x-axis: HEE to midpoint between MT1 and MT5

y-axis: perpendicular to plane with MT1, MT5, and HEE

z-axis: perpendicular to x-axis and y-axis

Shank Coordinate System – origin at KJC

y-axis: AJC to KJC

x-axis: perpendicular to plane containing AJC, KJC, and FBH

z-axis: perpendicular to x-axis and y-axis

Thigh Coordinate System – origin at HJC

y-axis: KJC to HJC

x-axis: perpendicular to plane containing HJC, LKNE, and MKNE

z-axis: perpendicular to x-axis and y-axis

Pelvis Coordinate System – origin at midpoint between LHJC and RHJC

y-axis: LBJC to midpoint between LHJC and RHJC

x-axis: perpendicular to the plane containing LHJC, RHJC, and LBJC

z-axis: perpendicular to x-axis and y-axis

Trunk (Thorax) Coordinate System – origin at the midpoint between CLAV and C7

y-axis: LBJC to midpoint between CLAV and C7

z-axis: perpendicular to plane with CLAV, C7, and LBJC

x-axis: perpendicular to z-axis and y-axis

Upper Arm Coordinate System – origin at SJC

y-axis: EJC to SJC

x-axis: perpendicular to plane containing LE, ME, and SJC

z-axis: perpendicular to x-axis and y-axis

Forearm Coordinate System – origin at WJC

y-axis: WJC to EJC

x-axis: perpendicular to plane containing ME, LE, and WJC

z-axis: perpendicular to x-axis and y-axis

11.2 Appendix B: Methods for Determining Hip and Shoulder Joint Centers

The two main types of joint center estimations are regression (predictive) methods and functional (coordinate transformation) methods. With these estimation methods, error can result from marker artifacts. The markers are not rigidly fixed to the segment. Relative motion occurs between the markers and the bone and between markers on the same segment. The accuracy of the motion capture system can also introduce error. The methods used and assumptions made in these methods greatly affect the accuracy of the estimated hip joint center locations (Ehrig et al., 2006).

Two commonly used regression methods come from the work of Davis et al. (1991) and Harrington et al. (2007), which use markers on the left and right anterior (L/RASIS) and posterior (L/RPSIS) superior iliac spines (L/RASIS) and other measured parameters. The regression equations developed by Davis et al. (1991) are used in the Plug In Gait model by Vicon (Los Angeles, CA) to calculate hip joint centers (all of the measurements and calculated joint centers locations should be in mm). Studies have shown these methods to be accurate within 1-3 cm for hip joint center locations (Ehrig et al., 2006; Harrington et al., 2007; Leardini et al., 1999). Disadvantages of regression techniques are that they require exact placement of the markers on the anatomical landmarks and subjects that fit the norms of the empirical data. Another assumption that is made in regression methods is pelvic symmetry (Harrington et al., 2007). Depending on the subject, pelvic symmetry may not be a good assumption.

Functional methods for determining hip joint centers include sphere fit methods and transformation techniques. Sphere fitting methods optimize the center and radii of spheres to fit the path of markers on one segment (femur segment) during its motion about another segment (pelvis segment). They assume that each femur marker moves on the surfaces of spheres with different radii and a common center at the hip center of rotation (CoR). They then determine the CoR and radii that best fit this marker data. The resulting CoR is the estimate of the hip joint center. One major assumption in these methods is that one of the segments is at rest and the CoR is stationary (Ehrig et al., 2006). Common sphere fitting techniques are the geometric (Capozzo, 1984; Ehrig et al., 2006), algebraic (Delonge, 1972; Gamage and Lasenby, 2002; Kasa, 1976), bias compensated algebraic (Halvorsen, 2003), and Pratt (Pratt, 1987) methods.

Transformation techniques define 3D local coordinate systems for the segments on one or both sides of the joint, assuming that the markers on each segment are fixed in relation to the other markers on the same segment. As the femur segment is moved relative to the pelvis, the CoR is calculated from the 3D coordinate systems. There are two types of transformation techniques: one-sided methods and two-sided methods. One-sided transformation techniques still use the assumption that one segment and the CoR are stationary, while two-sided transformation techniques allow for a moving CoR. One-sided methods include the center transformation technique (CTT) (Ehrig et al., 2006), the Holzreiter Approach (Holzreiter, 1991), the Schwartz method (Schwartz and Rozumalski, 2005), the Helical Pivot method (Woltring et al., 1985), the Minimal Amplitude Point Method (Marin et al., 2003), and the Stoddart approach (Stoddart et al., 1999). As error is introduced in assuming that one segment is at rest relative to the other, two-sided techniques have an advantage over the one-sided techniques. A two-sided technique that has been developed is the Symmetrical CoR Estimation (SCoRE) which has the ability to determine a moving CoR. Within a segment anatomical reference frame, the positions of the markers are assumed to remain constant relative to each other and to the segment. In the SCoRE method, local reference frames are assigned to the segments on each side of the joint and the global differences between the CoRs found in each local reference frame are minimized (Ehrig et al., 2006).

The functional methods have an advantage over regression methods in that they do not rely on empirical correlations or exact marker placement. The functional methods also allow more individualization than the regression methods do. Many studies have compared the functional methods with varying conclusions on the most accurate method for determining the hip joint center (Camomilla et al., 2006; Cereatti et al., 2009; Ehrig et al., 2006; Lopomo et al, 2010; MacWilliams, 2008; Sangeux et al., 2011). Overall, the algebraic method seemed to be the least accurate, while the geometric, bias compensated algebraic, and Pratt methods had similar accuracy (although the accuracy of the geometric method depended on a close initial estimate for the CoR). The bias compensated algebraic method was shown by a slight majority of the studies to have the best accuracy of the sphere fitting methods (Camomilla et al., 2006; Ehrig et al., 2006; Gamage and Lasenby, 2002; MacWilliams, 2008). In studies with one-sided segment motion, the SCoRE, CTT, Schwartz, Holzreiter and Helical Pivot techniques all had error very similar to the geometric, bias compensated algebraic, and Pratt sphere fit methods. In studies with motion of both segments, spherical fit methods showed much larger error, while the SCoRE, CTT, Schwartz, Holzreiter and Helical Pivot techniques still showed very similar error. The Minimal Amplitude Method and the Stoddart approach resulted in higher error than the other transformation techniques for both cases, particularly with lower ranges of motion (Ehrig et al., 2006).

Of the SCoRE, CTT, Schwartz, Holzreiter and Helical Pivot Techniques, SCoRE was chosen for the model in this study. The Helical Pivot and Schwartz methods are both accurate, but very computationally expensive and time-consuming (Camomilla et al., 2006; Ehrig et al., 2006). The CTT and Holtreitzer methods are simple, but assume that one segment is at rest and the CoR is stationary. The SCoRE method is both simple and accurate. It is a two-sided technique that is capable of calculating a moving CoR, which seems to have an advantage in practical applications. Also, the SCoRE method has shown more accurate results at lower ranges of motion than the sphere fit methods and some of the other transformation techniques, making it less dependent on the range of joint motion and specific motion used during data collection. One issue with using SCoRE is that it is more affected by relative motion between the markers than the spherical methods, which needs to be accounted for in the marker set and method chosen for data collection (Ehrig et al., 2006). The SCoRE method was therefore used to determine the hip joint centers, as well as the shoulder joint centers, for this study.

Preliminary testing was performed to check for accuracy of the model used in this study. The hip joint centers determined using the SCoRE method were compared to joint centers determined using common regression equations. The motion used for the SCoRE method was one cycle of a Star Arc movement which is similar to the FE/Abd/Circ movements used in this study. Seven flexion-extension/abduction-adduction movements from the neutral position to a 30° angle were performed, followed by a half circumduction motion with the hip at an angle of 30° (Camomilla et al., 2006). Joint centers using the Davis and both Harrington regression methods were calculated. A comparison was also made to the joint centers output from a regression model used by Mary Free Bed Rehabilitation Hospital in Grand Rapids, Michigan in their clinical gait lab that is based on the model by Seidel et al. (1995).

Table B-1 shows the resulting hip joint centers for the left and right sides. The results from the SCoRE method were close to many of the regression methods and seemed reasonable. In the x direction, all of the joint centers were within about 3 cm of each other, with the SCoRE and Harrington methods within 1.5 cm of each other. In the y direction, the hip joint centers were all within 1.5 cm of each other. In the z direction, all of the joint centers were also within about 1.5 cm of each other, except the ones from the Mary Free Bed model. The Mary Free Bed hip joint centers were about 3 cm higher in the z direction than the joint centers found with any of the other methods. While these results do not prove that the SCoRE method is accurate as the actual joint center is unknown, they do indicate that the SCoRE method results in similar joint centers to commonly used regression methods. The results suggest that the SCoRE method was an appropriate choice and was implemented correctly.

Table B-1: Comparison of Hip Joint Centers from Four Regression Methods and SCoRE.

Method	**RHJC (mm)**			**LHJC (mm)**		
	x	y	z	x	y	z
SCoRE	121	682	886	300	684	884
Harrington	111	680	895	304	683	889
Harringtion - Linear	119	680	893	294	683	887
Davis	127	669	881	286	672	876
Mary Free Bed	93	682	926	319	686	919

11.3 Appendix C: Rotation Matrices and Euler Angle Calculations

The XYZ Euler rotation sequence was used for all of the joint angles in this model. The angles were assigned as follows:

$\beta =$ Rotation about the x-axis (abduction/adduction, varus/valgus, inversion/eversion)

$\gamma =$ Rotation about the y-axis (internal/external rotation)

α = Rotation about the z-axis (flexion/extension or dorsiflexion/plantarflexion)

The rotation matrix for the joint angles was determined using equation C-1.

$$R_{joint} = R_{xyz} = [R_{z''}][R_{y'}][R_x] \tag{C-1}$$

The individual rotation matrices for each rotation about the axes are given in equations C-2 through C-3.

$$R_x = \begin{bmatrix} 1 & 0 & 0 \\ 0 & \cos\beta & \sin\beta \\ 0 & -\sin\beta & \cos\beta \end{bmatrix} \tag{C-2}$$

$$R_y = \begin{bmatrix} \cos\gamma & 0 & -\sin\gamma \\ 0 & 1 & 0 \\ \sin\gamma & 0 & \cos\gamma \end{bmatrix} \tag{C-3}$$

$$R_z = \begin{bmatrix} \cos\alpha & \sin\alpha & 0 \\ -\sin\alpha & \cos\alpha & 0 \\ 0 & 0 & 1 \end{bmatrix} \tag{C-4}$$

Multiplying the individual rotation matrices in equation C-1 results in the joint rotation matrix in equation C-5.

$$R_{joint} = \begin{bmatrix} \cos\alpha\cos\gamma & \cos\beta\sin\alpha + \cos\alpha\sin\beta\sin\gamma & \sin\alpha\sin\beta - \cos\alpha\cos\beta\sin\gamma \\ -\cos\gamma\sin\alpha & \cos\alpha\cos\beta - \sin\alpha\sin\beta\sin\gamma & \cos\alpha\sin\beta + \cos\beta\sin\alpha\sin\gamma \\ \sin\gamma & -\cos\gamma\sin\beta & \cos\beta\cos\gamma \end{bmatrix} \tag{C-5}$$

From the joint angle rotation matrix, the rotation angle about the y-axis (γ) was found using equation C-6. In the following equations, R_{ij} represents the component of the matrix in row i and column j.

$$\gamma = \sin^{-1}(R_{31}) \tag{C-6}$$

Using the result from equation C-6, the rotation angles about the x-axis (β) and the z-axis (α) can be calculated with equations C-7 and C-8, respectively.

$$\beta = \tan^{-1}\left(\frac{\frac{R_{32}}{-\cos(\gamma)}}{\frac{R_{33}}{\cos(\gamma)}}\right) \tag{C-7}$$

$$\alpha = \tan^{-1}\left(\frac{\frac{R_{21}}{-\cos(\gamma)}}{\frac{R_{11}}{\cos(\gamma)}}\right) \tag{C-8}$$

3D Angular Velocity in Segment Anatomical Reference Frames

The segment Euler angles were differentiated to determine the three non-orthogonal angular velocity components using equation C-9.

$$\dot{\theta}_i = \frac{\theta_{i+1} - \theta_{i-1}}{2\left(\frac{1}{fs}\right)} \tag{C-9}$$

To transform the vectors the segment anatomical reference frame, equation C-10 was used, along with the rotation matrices in equations C-2 to C-4.

$$\vec{\omega} = R_z \cdot R_y \cdot \begin{pmatrix} \dot{\beta} \\ 0 \\ 0 \end{pmatrix} + R_z \cdot \begin{pmatrix} 0 \\ \dot{\gamma} \\ 0 \end{pmatrix} + \begin{pmatrix} 0 \\ 0 \\ \dot{\alpha} \end{pmatrix} \tag{C-10}$$

The equations for each component of the angular velocity in the anatomic reference frame are given below:

$$\omega_x = \dot{\beta} \cos\alpha \cos\gamma + \dot{\gamma} \sin\alpha \tag{C-11}$$

$$\omega_y = -\dot{\beta} \sin\alpha \cos\gamma + \dot{\gamma} \cos\alpha \tag{C-12}$$

$$\omega_z = \dot{\alpha} + \dot{\beta} \sin\gamma \tag{C-13}$$

3D Angular Acceleration in Segment Anatomical Reference Frames

The segment Euler angles were differentiated twice to determine the three non-orthogonal angular acceleration components using equation C-14.

$$\ddot{\theta}_\iota = \frac{\theta_{i+1} - 2\theta_i + \theta_{i-1}}{\left(\frac{1}{fs}\right)^2} \tag{C-14}$$

The equations for each component of the angular acceleration in the anatomic reference frame were determined by differentiating angular velocity equations C-15 to C-17 as shown below:

$$\alpha_x = \ddot{\beta} \cos\alpha \cos\gamma + \ddot{\gamma} \sin\alpha - \dot{\alpha}\dot{\beta} \cos\gamma \sin\alpha - \dot{\gamma} \cos\alpha \, (\dot{\beta} \sin\gamma - \dot{\alpha}) \tag{C-15}$$

$$\alpha_y = -\ddot{\beta} \sin\alpha \cos\gamma + \ddot{\gamma} \cos\alpha - \dot{\alpha}\dot{\beta} \cos\gamma \cos\alpha - \dot{\gamma} \sin\alpha \, (\dot{\beta} \sin\gamma - \dot{\alpha}) \tag{C-16}$$

$$\alpha_z = \ddot{\beta} \, \dot{\gamma} \cos\gamma + \ddot{\beta} \sin\gamma \tag{C-17}$$